

1 **Mid-Holocene climate change over China: model-data discrepancy**

2 Yating Lin ^{1,2,4}, Gilles Ramstein ², Haibin Wu ^{1,3,4}, Raj Rani ², Pascale Braconnot ²,
3 Masa Kageyama ², Qin Li ^{1,3}, Yunli Luo ⁵, Ran Zhang ⁶ and Zhengtang Guo ^{1,3,4}

4 1. Key Laboratory of Cenozoic Geology and Environment, Institute of Geology and
5 Geophysics, Chinese Academy of Sciences, Beijing 100029, China

6 2. Laboratoire des Sciences du Climat et de l'Environnement, LSCE/IPSL,
7 CEA-CNRS-UVSQ, Université Paris-Saclay, Gif-sur-Yvette 91191, France

8 3. CAS Center for Excellence in Life and Paleoenvironment, Beijing, 100044, China

9 4. University of Chinese Academy of Sciences, Beijing 100049, China

10 5. Institute of Botany, Chinese Academy of Sciences, Beijing 100093, China

11 6. Institute of Atmospheric Physics, Chinese Academy of Sciences, Beijing 100029, China

12 **Abstract:**

13 The mid-Holocene period (MH) has long been an ideal target for the validation of Global
14 Circulation Model (GCM) results against reconstructions gathered in global datasets. These
15 studies aimed to test the GCM sensitivity mainly to the seasonal changes induced by the orbital
16 parameters (precession). Despite widespread agreement between model results and data on the
17 MH climate, some important differences still exist. There is no consensus on the continental
18 size of the MH thermal climate response, which makes regional quantitative reconstruction
19 critical to obtain a comprehensive understanding of the MH climate patterns. Here, we compare
20 the annual and seasonal outputs from the most recent Paleoclimate Modelling Intercomparison
21 Projects Phase 3 (PMIP3) models with an updated synthesis of climate reconstruction over
22 China, including, for the first time, a seasonal cycle of temperature and precipitation. Our
23 results indicate that the main discrepancies between model-data for MH climates are the annual
24 and winter mean temperature. A warmer-than-present climate condition are derived from
25 pollen data for both annual mean temperature (~0.7 K on average) and winter mean temperature

26 (~1 K on average), while most of the models provide a linear response driven by the seasonal
27 forcing (a decreased annual mean temperature with a warmer summer and colder winter). By
28 conducting simulations in BIOME4 and CESM version 1.0.5, we show that to capture the
29 seasonal pattern reconstructed by data, it is critical to assess surface processes. These results
30 pinpoint the crucial importance of including the non-linear of the surface water and energy
31 balance to vegetation changes.

32

33 *Keywords:* PMIP3 Pollen data Inverse Vegetation Model Seasonal climate change

34

35

36 **1. Introduction**

37 Much attention of paleoclimate study has been focused on the current interglacial (the
38 Holocene), especially the mid-Holocene (MH, 6 ± 0.5 ka). The major difference in the
39 experimental configuration between the MH and pre-Industrial (PI) arises from the orbital
40 parameters which brings about an increase in the amplitude of the seasonal cycle of insolation
41 of the Northern Hemisphere and a decrease in the Southern Hemisphere (Berger, 1978). Thus,
42 the MH provides an excellent case study on which to base an evaluation of the climate response
43 to changes in the distribution of insolation. Great efforts are devoted by the modeling
44 community to the design of the MH common experiments using similar boundary conditions
45 (Joussaume and Taylor, 1995; Harrison et al., 2002; Braconnot et al., 2007a, b). In addition,
46 much work has been done to reconstruct the paleoclimate change based on different proxies at
47 global and continental scale (Guiot et al., 1993; Kohfeld and Harrison, 2000; Prentice et al.,
48 2000; Bartlein et al., 2011). The greatest progress in understanding the MH climate change and

49 variability has consistently been made by comparing large-scale analyses of data with
50 simulations from global climate models (Joussaume et al., 1999; Liu et al., 2004; Harrison et al.,
51 2014).

52 However, the source of discrepancies between model and data is still an open and stimulating
53 question. Two types of inconsistencies have been identified: 1) where the model and data show
54 opposite signs, for instance, paleoclimate evidence from data-records indicates an increase of
55 about 0.5 K in global annual mean temperature during the MH compared with PI (Shakun et al.
56 2012; Marcott et al. 2013), while there is a cooling trend in model simulations (Liu et al., 2014).
57 2) where the same trend is displayed by both model and data but with different magnitudes.
58 Previous studies have shown that while climate models can successfully reproduce the direction
59 and large-scale patterns of past climate changes, they tend to consistently underestimate the
60 magnitude of change in the monsoons of the Northern Hemisphere as well as the amount of the
61 MH precipitation over northern Africa (Braconnot et al., 2012; Harrison et al., 2015). Moreover,
62 significant spatial variability has been noted in both observations and simulations (Peyron et al.
63 2000; Davis et al. 2003; Braconnot et al., 2007a; Wu et al. 2007; Bartlein et al. 2011), which
64 makes regional quantitative reconstruction (Davis et al., 2003; Mauri et al., 2015) essential to
65 obtain a comprehensive understanding of the MH climate patterns, and to act as a benchmark to
66 evaluate climate models (Fischer and Jungclaus, 2011; Harrison et al., 2014;).

67 China offers two advantages in respect to these issues. The sheer expanse of the country
68 means that the continental response to insolation changes over a large region can be
69 investigated. Moreover, the quantitative reconstruction of seasonal climate changes during the
70 MH, based on the new pollen dataset, provides a unique opportunity to compare the seasonal
71 cycles for models and data. Previous studies indicate that warmer and wetter than present
72 conditions prevailed over China during the MH and that the magnitude of the annual
73 temperature increases varied from 2.4-5.8 K spatially, with an annual precipitation increase in

74 the range of 34-267 mm (e.g., Sun et al., 1996; Jiang et al., 2010; Lu et al., 2012; Chen et al.,
75 2015). However, Jiang et al. (2012) clearly show a mismatch between multi-proxy
76 reconstructions and model simulations. In terms of climate anomalies (MH-PI), besides the ~1
77 K increase in summer temperature, 35 out of 36 Paleoclimate Modelling and Coupled
78 Modelling Intercomparison Projects (PMIP) models reproduce annual (~0.4 K) and winter
79 temperatures (~1.4 K) that are colder than the baseline, and a drier-than-baseline climate in
80 some western and middle regions over China is depicted in models (Jiang et al. 2013).Jiang et
81 al. (2012) were the first to point out the model-data discrepancy over China during the MH,
82 but the lack of seasonal reconstructions in their study limits comparisons with simulations..

83 An important issue raised by Liu et al. (2014) is that the discrepancy at the annual level could
84 be due to incorrect reconstructions of the seasonal cycle, a key objective in our paper. Moreover,
85 it has been suggested that the vegetation change can strengthen the temperature response in
86 high latitudes (O’Ishi et al., 2009; Otto et al., 2009), as well as alter the hydrological conditions
87 in the tropics (Liu et al., 2007). However, compared to the substantial land cover changes in the
88 MH derived from pollen datasets (Ni et al., 2010; Yu et al., 2000), the changes in vegetation
89 have not yet been fully quantified and discussed in PMIP3 (Tylor et al., 2012).

90 In this study, for the reconstruction, we firstly used the quantitative method of biomization to
91 reconstruct vegetation types during the MH based on a new synthesis of pollen datasets, and
92 then used the Inverse Vegetation Model (Guiot et al. 2000; Wu et al. 2007) to obtain the annual,
93 the mean temperature of the warmest month (MTWA) and the mean temperature of the coldest
94 month (MTCO) climate features over China for the MH. In the case of PMIP3 models, we
95 present a comprehensive evaluation of the state-of-the-art models based on the MH climate
96 variables (vegetation, temperature and precipitation), using the simulations from the PMIP3.
97 This is the first time that such progress towards a quantitative seasonal climate comparison for
98 the MH over China has been made, thanks to the seasonal reconstruction and the PMIP3 results.

99 This point is crucial because the MH PMIP3 experiment is essentially one that looks at the
100 response of the models to changes in the seasonality of insolation, and the attempt to derive
101 reconstructions of both summer and winter climate to compare with the simulations will thus be
102 able to answer the question posed by Liu et al. (2014) on the importance of seasonal
103 reconstruction.

104 **2. Data and Methodology**

105 **2.1 Data**

106 In this study, we collected 159 pollen records, covering most of China, for the MH period
107 (6000 ± 500 ^{14}C yr BP) (Fig. 1). Of these, 65 were from the Chinese Quaternary Pollen Database
108 (CQPD, 2000), three were original datasets obtained in our study, and the others were digitized
109 from pollen diagrams in published papers with a recalculation of pollen percentages based on
110 the total number of terrestrial pollen types. These digitized 91 pollen records were selected
111 according to three criteria: (1) clearly readable pollen diagrams with a reliable chronology with
112 the minimum of three independent age control points since the LGM; (2) including the pollen
113 taxa during 6000 ± 500 ^{14}C yr BP period with a minimum sampling resolution of 1000 years per
114 sample; (3) abandon the pollen records if the published paper mentions the influence of human
115 activity. The age-depth model for the pollen records was estimated by linear interpolation
116 between adjacent available dates or by regression. Using ranking schemes from the
117 Cooperative Holocene Mapping Project, the quality of dating control for the mid-Holocene was
118 assessed by assigning a rank from 1 to 7. And 70% of the records fell into the first and second
119 classes (see Table 1 for detailed information) according to the Webb 1-7 standards (Webb, T.
120 III, 1985). Vegetation type was quantitatively reconstructed using biomization (Prentice et al.,
121 1996), following the classification of plant functional types (PFTs) and biome assignment in

122 China by the Members of China Quaternary Pollen Data (CQPD, 2000), which has been widely
123 tested in surface sediment. The new sites (91 digitized data and three original data) added to our
124 database improved the spatial coverage of pollen records, especially in the northwest, the
125 Tibetan Plateau, the Loess Plateau and southern regions, where the data in the previous
126 databases are very limited.

127 Modern monthly mean climate variables, including temperature, precipitation and cloudiness
128 (means the cloud area fraction) have been collected for each modern pollen site based on the
129 datasets (1951-2001) from 657 meteorological observation stations over China (data source:
130 China Climate Bureau, China Ground Meteorological Record Monthly Report, 1951-2001).
131 Soil properties were derived from the digital world soil map produced by the Food and
132 Agricultural organization (FAO) (FAO, 1991), and, because of a lack of paleosol data, soil
133 characteristics were assumed to have been the same during the MH. Atmospheric CO₂
134 concentration for the MH was taken from ice core records (EPICA community members 2004),
135 and set at 270 ppmv.

136 A 3-layer back-propagation (BP) artificial neural network technique (ANN) was used for
137 interpolation on each pollen site (Caudill and Butler, 1992). Five input variables (latitude,
138 longitude, elevation, annual precipitation, annual temperature) and one output variable (biome
139 scores) have been chosen in ANN for the modern vegetation. The ANN has been calibrated on
140 the training set, and its performance has been evaluated on the verification set (20%, randomly
141 extracted from the total sets). After a series of training run, the lowest verification error is
142 obtained with 5 neurons in the hidden layer after 10000 iterations. The anomalies between past
143 (6ka) and modern vegetation indices (biome scores) was then interpolated to the 0.2 × 0.2 ° grid
144 resolution by applying the ANN. After that, the modern grid values are added to the values of
145 the grid of palaeo-anomalies to provide gridded paleo-biome indices. Finally, the biome with
146 the highest index is attributed to each grid point. This ANN method is more efficient than many

147 other techniques on condition that the results are validated by independent data sets, and
148 therefore, it has been widely applied in paleoclimatology (Guiot et al., 1996; Peyron et al.,
149 1998).

150 **2.2 Climate models**

151 PMIP, a long-standing initiative, is a climate-model evaluation project which provides an
152 efficient mechanism for using global climate models to simulate climate anomalies in the past
153 periods and to understand the role of climate feedback. In its third phase (PMIP3), the models
154 were identical to those used in the Climate Modelling Intercomparison Project 5 (CMIP5)
155 experiments. The experimental set-up for the mid-Holocene simulations in PMIP3 followed the
156 PMIP protocol (Braconnot et al. 2007a, b, 2012). The main forcing between the MH and PI in
157 PMIP3 are the orbital configuration and CH₄ concentration. More precisely, the orbital
158 configuration in the MH climate has an increased summer insolation and a decreased winter
159 insolation in the Northern Hemisphere compared to the PI climate (Berger, 1978). Meantime,
160 the CH₄ concentration is prescribed at 650 ppbv in the MH, while it is set at 760 ppbv in PI
161 (Table 2).

162 All 13 models (Table 3) from PMIP3 that have the MH simulation have been included in
163 our study, including eight ocean-atmosphere (OA) models and five
164 ocean-atmosphere-vegetation (OAV) models. Means for the last 30 years were calculated from
165 the archived time-series data on individual model grids for climate variables: near surface
166 temperature and precipitation flux, which were bi-linearly interpolated to a uniform 2.5 ° grid,
167 in order to get the bioclimatic variables (e.g. MAT, MAP, MTWM, MTCO, July precipitation)
168 onto a common grid for comparison with the reconstruction results.

169 **2.3 Vegetation model**

170 The vegetation model, BIOME4 is a coupled biogeography and biogeochemistry model
171 developed by Kaplan et al. (2003). Monthly mean temperature, precipitation, sunshine
172 percentage (–an inverse measure of cloud area fraction), absolute minimum temperature,
173 atmospheric CO₂ concentration and subsidiary information about the soil’s physical properties
174 like water retention capacity and percolation rates are the main input variables for the models. It
175 incorporates 13 plant functional types (PFTs), which have different bioclimatic limits. The
176 PFTs are based on physiological attributes and bioclimatic tolerance limits such as heat,
177 moisture and chilling requirements and resistance of plants to cold. These limits determine the
178 areas where the PFTs could grow in a given climate. A viable combination of these PFTs
179 defines a particular biome among 28 potential options. These 28 biomes can be further
180 classified into 8 megabiomes (Table S1). BIOME4 has been widely utilized to analyze the past,
181 present and potential future vegetation patterns (e.g. Bigelow et al., 2003; Diffenbaugh et al.,
182 2003; Song et al., 2005). In this study, we conducted 13 PI and the MH biome simulations using
183 PIMP3/CMIP5 climate fields (temperature, precipitation and sunshine) as inputs. The climate
184 fields, obtained from PMIP3/CMIP5, are the monthly mean data of the last 30 model years.

185 **2.4 Statistics and interpolation for vegetation distribution**

186 To quantify the differences between simulated (by the climate-model output) and
187 reconstructed (from pollen) between megabiomes, a map-based statistic (point-to-point
188 comparison with observations) called ΔV (Sykes et al., 1999; Ni et al., 2000) was applied to
189 our study. ΔV is based on the relative abundance of different plant life forms (e.g. trees, grass,
190 bare ground) and a series of attributes (e. g. evergreen, needle-leaf, tropical, boreal) for each
191 vegetation class. The definitions and attributes of each plant form follow naturally from the
192 BIOME4 structure and the vegetation attribute values in the ΔV computation were defined for

193 BIOME4 in the same way as for BIOME1 (Sykes et al., 1999). The abundance and attribute
194 values are given in Table 4 and Table 5, which describe the typical floristic composition of the
195 biomes. Weighting the attributes is subjective because there is no obvious theoretical basis for
196 assigning relative significance. Transitions between highly dissimilar megabiomes have a
197 weighting of close to 1, whereas transitions between less dissimilar megabiomes are assigned
198 smaller values. The overall dissimilarity between model and data megabiome maps was
199 calculated by averaging the ΔV for the grids with pollen data, while the value was set at 0 for
200 any grid without data. ΔV values < 0.15 can be considered to point to very good agreement
201 between simulated and actual distributions, 0.15-0.30 is good, 0.30-0.45 fair, 0.45-0.60 poor,
202 and > 0.80 very poor (adjusted from Zhang et al., 2010). For spatial pattern comparison, we
203 compared the simulated vegetation distribution from BIOME4 from each model with the
204 interpolated pattern.

205 **2.5 Inverse vegetation model**

206 Inverse Vegetation Model (Guiot et al., 2000; Wu et al. 2007), highly dependent on the
207 BIOME4 model, is applied to our reconstruction. The key concept of this model can be
208 summarized in two points: firstly, a set of transfer functions able to transform the model output
209 into values directly comparable with pollen data is defined. There is not full compatibility
210 between the biome typology of BIOME4 and the biome typology of pollen data. A transfer
211 matrix (Table S2) was defined in our study where each BIOME4 vegetation type is assigned a
212 vector of values, one of each pollen vegetation type, ranging from 0 (representing an
213 incompatibility between BIOME4 type and pollen biome type) to 15 (corresponding to a
214 maximum compatibility). Secondly, using an iterative approach, a representative set of climate
215 scenarios compatible with the vegetation records is identified among the climate space,
216 constructed by systematically perturbing the input variables (e.g. ΔT , ΔP) of the model (Table
217 S3).

218 Inverse Vegetation Model (IVM) provides a possibility, for the first time, to reconstruct both
219 annual and seasonal climates for the MH over China. Moreover, it offers a way to consider the
220 impact of CO₂ concentration on competition between PFTs as well as on the relative abundance
221 of taxa, and thus make reconstruction from pollen records more reliable. More detailed
222 information about IVM can be found in Wu et al. (2007).

223 We applied the inverse model to modern pollen samples to validate the approach by
224 reconstructing the modern climate at each site and comparing it with the observed values. The
225 high correlation coefficients (R=0.75–0.95), intercepts close to 0 (except for the mean
226 temperature of the warmest month), and slopes close to 1 (except for the July precipitation)
227 demonstrated that the inversion method worked well for most variables in China (see Table 6).

228 **3. Results**

229 **3.1 Comparison of annual and seasonal climate changes at the MH**

230 In this study, we collected 159 pollen records, broadly covering the whole of China (Fig. 1).
231 To check the reliability of the collected data, we first categorized our pollen records into
232 megabiomes in line with the standard tables developed for the BIOME6000 (Table S1), and
233 compared them with the BIOME6000 dataset (Fig.2). The match between collected data and
234 the BIOME6000 is more than 90% for both the MH and PI.

235 Based on pollen records, the spatial pattern of climate changes over China during the MH,
236 deduced from IVM, are presented in Fig. 3 (left panel, points), alongside the results from
237 PMIP3 models (shaded in Fig. 3). For temperature, a warmer-than-present annual climate
238 condition (~0.7 K on average) is derived from pollen data (the points in Fig. 3a), with the
239 largest increase occurring in the northeast (3-5 K) and a decrease in the northwest and on
240 Tibetan Plateau. On the other hand, the results from a multi-model ensemble (MME) indicate a
241 colder annual temperature generally (~-0.4 K on average), with significant cooling in the south

242 and slight warming in the northeast (shaded in Fig. 3a). Of the 13 models, 11 simulate a cooler
243 annual temperature compared with PI as MME. However, two models (HadeGEM2-ES and
244 CNRM-CM5) present the same warmer condition as was found in the reconstruction (Fig. 3d).
245 Compared to the reconstruction, the annual mean temperature during the MH is largely
246 underestimated by most PMIP3 models, which depict an anomaly ranging from ~ -1.4 to ~ -0.5 K.
247 Detailed information of reconstructed climate change derived from IVM at each pollen site can
248 be found in Table S4.

249 Concerning seasonal change, during the MH, MTWA from the data is ~ 0.5 K higher than PI,
250 with the largest increase in the northeast and a decrease in the northwest. From model outputs,
251 an average increase of ~ 1.2 K is reproduced by MME, with a more pronounced warming at high
252 latitudes which is consistent with the insolation change (Berger, 1978). Fig. 3e shows that all 13
253 models reproduce the same warmer summer temperatures as the data, and that HadGEM2-ES
254 and CNRM-CM5, reproduce the largest increases among the models. Although the warmer
255 MTWA is consistent between the models and data, there is a discrepancy between them on
256 MTCO. In Fig. 3c, the data show an overall increase of ~ 1 K, with the largest increase occurring
257 in the northeast and a decrease of opposite magnitude on the Tibetan Plateau. Inversely, MME
258 reproduces a decreased MTCO with an average amplitude of ~ -1.3 K, the coolest areas being
259 the southeast, the Loess Plateau and the northwest. Similarly to the MME, all 13 models
260 simulate a colder-than-present climate with amplitudes ranging from ~ -2.0 K (CCSM4 and
261 FGOALS-g2) to ~ -0.7 K (HadGEM2-ES and CNRM-CM5).

262 Concerning annual change in precipitation, the reconstruction shows wetter conditions
263 during the MH across almost the whole of China with the exception of part of the northwest.
264 The southeast presents the largest increase in annual precipitation. All but 2 models depict
265 wetter conditions with an amplitude of ~ 10 mm to ~ 70 mm. The reconstruction and MME
266 results also indicate an increased annual precipitation during MH (Fig.4a), with a much larger

267 magnitude visible in the reconstruction (~30 mm, ~230 mm respectively). The main
268 discrepancy in annual precipitation between simulations and reconstruction occurs in the
269 northeast, which is depicted as drier by the models and wetter by the data. With regard to
270 seasonal change, the reconstruction shows an overall increase in July rainfall (~50 mm on
271 average), with a decrease in the northwestern regions and east monsoon region at Yangtze
272 River valley. In line with the reconstruction, the MME also shows an overall increase in rainfall
273 (~13 mm on average), with a decrease in the northwest for July (Fig.4b). Notably, a much
274 larger increase is simulated for the south and the Tibetan Plateau by the models, while the
275 opposite pattern emerges along the eastern margin from both models and data. More detailed
276 information about the geographic distribution of simulated temperature and precipitation for
277 each model can be found in Fig. S1-S6.

278

279 **3.2 Comparison of vegetation change at the MH**

280 The use of the PMIP3 database is clearly limited by the different vegetation inputs among the
281 models for the MH period (Table S5). Only HadGEM2-ES and HadGEM2-CC use a dynamic
282 vegetation for the MH, and the other 11 models are prescribed to PI with or without interactive
283 LAI, which would introduce a bias to the role of vegetation-atmosphere interaction in the MH
284 climates. To evaluate the model results against the reconstruction for the MH vegetation, we
285 conducted 13 biome simulations in BIOME4 using PIMP3 climate fields, and the megabiome
286 distribution for each model during the MH is displayed in Fig. 5 (see Fig. S7 for PI vegetation
287 comparison). To quantify the model-data dissimilarity between megabiomes, a map-based
288 statistic called ΔV (Sykes et al., 1999; Ni et al., 2000) was applied here (detailed information is
289 in the methodology section).

290 Fig. S8 shows the dissimilarity between simulations and observations for megabiomes
291 during the MH, with the overall values for ΔV ranging from 0.43 (HadGEM2-ES) to 0.55

292 (IPSL-CM5A-LR). According to the classification of ΔV (see in the methodology section) for
293 the 13 models, 12 (all except HadGEM2-ES) showed poor agreement with the observed
294 vegetation distribution. Most models poorly simulate the desert, grassland and tropical forest
295 areas for both periods, but perform better for warm mixed forest, tundra and temperate forest.
296 However, this statistic is based on a point-to-point comparison and so the ΔV calculated here
297 cannot represent an estimation of full vegetation simulation due to the uneven distribution of
298 pollen data and the potentially huge difference in area of each megabiome. For instance, tundra
299 in our data for PI is represented by only 4 points, which counts for a small contribution to the
300 ΔV since we averaged it over a total of 159 points, but this calculation could induce a
301 significant bias if these 4 points cover a large area of China.

302 So, we used the biome scores based on the artificial neural network technique as described by
303 Guiot et al. (1996) for interpolation (the plots in red rectangle in Fig. 5), and compared the
304 simulated vegetation distribution from BIOME4 for each model with the interpolated pattern.
305 During the MH, most models are able to capture the tundra on the Tibetan Plateau as well as the
306 combination of warm mixed forest and temperate forest in the southeast. However, all models
307 fail to simulate or underestimate the desert area in the northwest compared to reconstructed data.
308 The main model-data inconsistency in the MH vegetation distribution occurs in the northeast,
309 where data show a mix of grassland and temperate forest, and the models show a mix of
310 grassland and boreal forest.

311 The area statistic carried out for simulated vegetation changes (Fig. 6) reveals that the main
312 difference during the MH, compared with PI, is that grassland replaced boreal forest in large
313 tracts of the northeast (Fig. 5, Fig. S7). No other significant difference in vegetation distribution
314 between the two periods was derived from models. Unlike in models, three main changes in
315 megabiomes during the MH are depicted by the data. Firstly, the megabiomes converted from
316 grassland to temperate forest in the northeast. Secondly, a large area of temperate forest was

317 replaced in the southeast by a northward expansion of warm mixed forest. Thirdly, in the
318 northwest and at the northern margin of the Tibetan Plateau, part of the desert area changed into
319 grassland. However, none of the models succeed in capturing these features, especially the
320 transition from grassland into forest in the northeast during the MH. Therefore, this failure to
321 capture vegetation changes between the two periods will lead to a cumulating inconsistency in
322 the model-data comparison for climate anomalies because of the vegetation-climate feedbacks.

323 **4. Conclusion and Discussion**

324 In response to the seasonal insolation change prescribed in PMIP3 for the MH, all models
325 produce similar large-scale patterns for seasonal temperature and precipitation (higher than
326 present July precipitation and MTWA, lower than present MTCO), with either an over- or
327 underestimate of the climate changes when compared to the data. The main discrepancy
328 emerging from the model-data comparison occurs in the annual and MTCO, where data show
329 an increased value and most models simulate the opposite except CNRM-CM5 and
330 HadGEM2-ES reproduced the higher-than-present annual temperature during MH as data
331 showed. Besides the qualitative consistency among models, caused by the protocol of –PMIP3
332 experiments (Table 2), a variability in the magnitude of anomalies between models is clearly
333 illustrated by the column bars (Fig.3 and Fig.4). These disparities in value or even pattern
334 among models reflect the obvious differences in the response by the climate models to the MH
335 forcing which raises on the question of the magnitude of feedbacks among models.

336 As positive feedbacks between climate and vegetation are important to explain regional
337 climate changes, the failure to capture or the underestimation of the amplitude and pattern of
338 the observed vegetation differences among models (see Section 3.2) could amplify and partly
339 account for the model-data disparities in climate change, mainly due to variations in the albedo.
340 Because the HadGEM2-ES and HadGEM2-CC are the only two models in PMIP3 with

341 dynamic vegetation simulation for the MH, we thus focused on them to examine the variations
342 in vegetation fraction in the simulations. The main vegetation changes during the MH
343 demonstrated by HadGEM2-ES are increased tree coverage (~15%) and a decreased bare soil
344 fraction (~6%), while HadGEM2-CC depicts a ~3% decrease in tree fraction and a ~1%
345 increase in bare soil (Fig. S9). We made a rough calculation of albedo variance caused solely by
346 vegetation change for both two models and for our reconstruction, based on the area fraction
347 and albedo value of each vegetation type (Betts, 2000; Bonfils et al., 2001; Oguntunde et al.,
348 2006; Bonan, 2008).

349 Reconstruction showed vegetation changes during the MH leading to a ~1.8% decrease in
350 albedo when snow-free, with a much larger impact (~4.2% decrease) when snow-covered. The
351 results from HadGEM2-ES are highly consistent with the albedo changes from the
352 reconstruction, featuring a ~1.4% (~6.5%) decrease without (with) snow, while HadGEM2-CC
353 produces an increased albedo value during the MH (~0.22% for snow-free, ~1.9% with
354 snow-cover), depending on its vegetation simulation. Two ideas could be inferred from this
355 calculation, 1) HadGEM2-ES is much better in simulating the MH vegetation changes than
356 HadGEM2-CC. 2) the failure by models to capture these vegetation changes will result in a
357 much larger impact on winter albedo (with snow) than summer albedo (without snow).

358 These surface albedo changes due to vegetation changes could have a cumulative effect on
359 the regional climate by modifying the radiative fluxes. For instance, the spread of trees into the
360 grassland biome in the northeast during the MH, revealed by the reconstruction in our study,
361 should act as a positive feedback to climate warming by increasing the surface net shortwave
362 radiation associated with reductions in albedo due to taller and darker canopies (Chapin et al.,
363 2005). Previous studies show that cloud and surface albedo feedbacks on radiation are major
364 drivers of differences between model outputs for past climates. Moreover, the land surface
365 feedback shows large disparities among models (Braconnot and Kageyama, 2015).

366 We used a simplified approach (Taylor et al., 2007) to quantify the feedbacks and to compare
367 model behavior for the MH, thus justifying the focus on surface albedo and atmospheric
368 scattering (mainly accounting for cloud change). Surface albedo and cloud change are
369 calculated using the simulated incoming and outgoing radiative fluxes at the Earth's surface
370 and at the top of atmosphere (TOA), based on data for the last 30 years averaged from all
371 models. Using this framework, we quantified the effect of changes in albedo on the net
372 shortwave flux at TOA (Braconnot and Kageyama, 2015), and further investigated the
373 relationship between these changes and temperature change. Fig.7 shows that most models
374 produced a negative cloud cover and surface albedo feedback on the annual mean shortwave
375 radiative forcing. Concerning seasonal change, the shortwave cloud and surface feedback in
376 most models tend to counteract the insolation forcing during the boreal summer, while they
377 enhance the solar forcing during winter. A strong positive correlation between albedo feedback
378 and temperature change is depicted, with a large spread in the models owing to the difference in
379 albedo in the 13 models. In particular, CNRM-CM5 and HadGEM2-ES capture higher values
380 of cloud and surface albedo feedback, which could be the reason for the reversal of the
381 decreased annual temperature seen in other models (Fig. 3d).

382 However, the vegetation patterns produced by BIOME4 in Fig. 5 are not used in PMIP3
383 experiment setup, it's actually determined by the input variables from models. To better
384 quantify the vegetation-climate feedback, two experiments were conducted in CESM version
385 1.0.5, including a mid-Holocene (MH) experiment (6 ka) with original vegetation setting
386 (prescribed as PI vegetation for MH) and a MH experiment with reconstructed vegetation (6
387 ka_VEG). Fig. 8 shows the climate anomalies (6 ka_VEG minus 6 ka) between two
388 simulations, for both annual and seasonal scale. For temperature, it's clear that the 6 ka_VEG
389 simulation reproduces the warmer annual (~ 0.3 K on average) and winter temperature (~ 0.6 K
390 on average), especially the winter temperature. For precipitation, the reconstructed vegetation

391 leads to higher annual and seasonal precipitation, which can also reconcile the discrepancy of
392 increase amplitude for precipitation during MH between model-data (data reproduced larger
393 amplitude than model, revealed by our study). So the mismatch between model-data in MH
394 vegetation could partly account for the discrepancy of climate due to the interaction between
395 vegetation and climate through radiative and hydrological forcing with albedo. These results
396 pinpoint the value of building a new generation of models able to capture not only the
397 atmosphere and ocean response, but also the non-linear responses of vegetation and hydrology.
398 Moreover, besides the vegetation influence, to which extent this model-data discrepancy is
399 related to rough topography, soil type and other possible factors should be investigated in the
400 future work.

401 Besides the uncertainties in the models, IVM, from the data perspective, relies heavily on
402 BIOME4, and since BIOME4 is a global vegetation model, it is possible that the spatial
403 robustness of regional reconstruction could be less than that of global reconstruction due to the
404 failure to simulate local features (Bartlein et al., 2011). China, located in the Asian monsoon
405 area, has some specialized vegetation types which call for an improved ability to simulate
406 regional vegetation in BIOME4. Moreover, the output of the model is not directly compared to
407 the pollen data, the conversion of BIOME4 biomes to pollen biomes by the transfer matrix
408 may add the source of uncertainty in reconstruction. All these bias in reconstruction should
409 also be considered in the discrepancy between model-data for climate change during MH over
410 China. Of course, more reconstruction studies using multiple proxies and reliable methods are
411 also required to narrow the discrepancies between data and model results.

412 **Data availability**

413 The PMIP3 output is publicly available at website (<http://pmip3.lsce.ipsl.fr/>) by the climate
414 modelling groups, the 65 pollen biomization results are provided by Members of China

415 Quaternary Pollen Data Base, Table 1 shows the information (including references) of the 91
416 collected pollen records and 3 original ones in our study. All the reconstructed climate values
417 at each pollen site from IVM are provided in Table S4. The full datasets of pollen are
418 available upon the request to the corresponding author.

419 **Author contribution**

420 Yating Lin carried out the model-data analysis and prepared for the first manuscript, Gilles
421 Ramstein contributed a lot to the paper's structure and content, Haibin Wu provided the
422 reconstruction results from IVM and contributed the paper's structure and content. Raj
423 Rani-Singh conducted the BIOME4 simulations. Pascale Braconnot, Masa Kegeyama and
424 Zhengtang Guo contributed great ideas on model-data comparison work. Qin Li and Yunli Luo
425 provided pollen data. All co-authors helped to improve the paper.

426 **Competing interest**

427 The authors declare no competing interests.

428 **Acknowledgements**

429 We acknowledge the World Climate Research Program's Working Group on Coupled
430 Modelling, which is responsible for PMIP/CMIP, and we thank the climate modelling groups
431 for producing and making available their model output. This research was funded by the
432 Sino-French Caiyuanpei Program, the National Basic Research Program of China (Grant no.
433 2016YFA0600504), the National Natural Science Foundation of China (Grant nos. 41572165,
434 41690114, and 41125011), and the Bairen Programs of the Chinese Academy of Sciences.

435 **References**

- 436 An, C., Zhao, J., Tao, S., Lv, Y., Dong, W., Li, H., Jin, M., and Wang, Z.: Dust variation
437 recorded by lacustrine sediments from arid Central Asia since ~ 15 cal ka BP and its
438 implication for atmospheric circulation, *Quaternary Research*, 75, 566-573, 2011.
- 439 Bao, Q., Lin, P., Zhou, T., Liu, Y., Yu, Y., Wu, G., He, B., He, J., Li, L., Li, J., Li, Y., Liu, H.,
440 Qiao, F., Song, Z., Wang, B., Wang, J., Wang, P., Wang, X., Wang, Z., Wu, B., Wu, T.,
441 Xu, Y., Yu, H., Zhao, W., Zheng, W., and Zhou, L.: The flexible global
442 oceanatmosphere-land system model, spectral version 2: FGOALS-s2. *Adv. Atmos. Sci.*,
443 30, 561-576, 2013.
- 444 Bartlein, P. J., Harrison, S. P., Brewer, S., Connor, S., Davis, B. A. S., Gajewski, K., Guiot, J.,
445 Harrison-Prentice, T. I., Henderson, A., Peyron, O., Prentice, I. C., Scholze, M., Seppä H.,
446 Shuman, B., Sugita, S., Thompson, R. S., Viau, A. E., Williams, J., and Wu, H.B.:
447 Pollen-based continental climate reconstructions at 6 and 21ka: a global synthesis, *Climate*
448 *Dynamics*, 37, 775-802, 2011.
- 449 Berger, A.: Long-Term Variations of Daily Insolation and Quaternary Climatic Changes,
450 *Journal of the Atmospheric Sciences*, 35, 2362-2367, 1978.
- 451 Betts, R. A.: Offset of the potential carbon sink from boreal forestation by decreases in surface
452 albedo, *Nature*, 408, doi: 10.1038/nature.35041545, 2000.
- 453 Bigelow, N. H., Brubaker, L. B., Edwards, M. E., Harrison, S. P., Prentice, I. C., Anderson, P.
454 M., Andreev, A. A., Bartlein, P. J., Christensen, T. R., Cramer, W., Kaplan, J. O., Lozhkin,
455 A. V., Matveyeva, N. V., Murray, D. F., David McGuire, A., Razzhivin, V. Y., Ritchie, J. C.,
456 Smith, B., Walker, A. D., Gajewski, K., Wolf, V., Holmqvist, B. H., Igarashi, Y.,
457 Kremenetskii, K., Paus, A., Pisaric, M. F. J., and Volkova, V. S.: Climate change and Arctic

458 ecosystems: 1. Vegetation changes north of 55 °N between the last glacial maximum,
459 mid-Holocene and present, *Journal of Geophysical Research*, 108, 1-25, 2003.

460 Bonan, G. B.: Forests and Climate Change: Forcings, Feedbacks, and the Climate Benefits of
461 Forests, *Science*, 320, 1444-1449, 2008.

462 Bonfils, C., de Noblet-Ducoudré N, Braconnot, P., and Joussaume, S.: Hot Desert Albedo and
463 Climate Change: Mid-Holocene Monsoon in North Africa, *Journal of Climate*, 14,
464 3724–3737, 2001.

465 Braconnot, P., and Kageyama, M.: Shortwave forcing and feedbacks in Last Glacial Maximum
466 and Mid-Holocene PMIP3 simulations, *Philosophical Transactions of the Royal Society A:
467 Mathematical, Physical and Engineering Sciences*, 373, 2054-2060, 2015.

468 Braconnot, P., Harrison, S. P., Kageyama, M., Bartlein, P. J., Masson-Delmotte, V., Abe-Ouchi,
469 A., Otto-Bliesner, B., and Zhao, Y.: Evaluation of climate models using palaeoclimatic data:
470 *Nature Climate Change*, 2, 417-421, 2012.

471 Braconnot, P., Otto-Bliesner, B., Harrison, S., Joussaume, S., Peterchmitt, J. Y., Abe-Ouchi, A.,
472 Crucifix, M., Driesschaert, E., Fichefet, T., Hewitt, C. D., Kageyama, M., Kitoh, A., Laine,
473 A., Loutre, M. F., Marti, O., Merkel, U., Ramstein, G., Valdes, P., Weber, S. L., Yu, Y., and
474 Zhao, Y.: Results of PMIP2 coupled simulations of the Mid-Holocene and Last Glacial
475 Maximum-Part 1: experiments and large-scale features, *Clim. Past*, 3, 261-277, 2007a.

476 Braconnot, P., Otto-Bliesner, B., Harrison, S., Joussaume, S., Peterschmitt, J. Y., Abe-Ouchi,
477 A., Crucifix, M., Driesschaert, E., Fichefet, T., Hewitt, C. D., Kageyama, M., Kitoh, A.,
478 Loutre, M. F., Marti, O., Merkel, U., Ramstein, G., Valdes, P., Weber, L., Yu, Y., and Zhao,
479 Y.: Results of PMIP2 coupled simulations of the Mid-Holocene and Last Glacial
480 Maximum-Part 2: feedbacks with emphasis on the location of the ITCZ and mid- and high
481 latitudes heat budget, *Clim. Past*, 3, 279-296, 2007b.

482 Cai, Y.: Study on environmental change in Zoige Plateau: Evidence from the vegetation
483 record since 24000a B.P., Chinese Academy of Geological Sciences, Mater Dissertation,
484 2008 (in Chinese).

485 Caudill, M., Bulter, C.: Understanding Neural Networks, Basic Networks, 1, 309, 1992.

486 Chapin, F. S., Sturm, M., Serreze, M. C., McFadden, J. P., Key, J. R., Lloyd, A. H.,
487 McGuire, A. D., Rupp, T. S., Lynch, A. H., Schimel, J. P., Beringer, J., Chapman, W. L.,
488 Epstein, H. E., Euskirchen, E. S., Hinzman, L. D., Jia, G., Ping, C.L., Tape, K. D.,
489 Thompson, C. D. C., Walker, D. A., and Welker, J. M.: Role of Land-Surface Changes in
490 Arctic Summer Warming, *Science*, 310, 657-660, 2005.

491 Chen, F., Cheng, B., Zhao, Y., Zhu, Y., and Madsen, D. B.: Holocene environmental change
492 inferred from a high-resolution pollen record, Lake Zhuyeze, arid China, *The Holocene*, 16,
493 675-684, 2006.

494 Chen, F., Xu, Q., Chen, J., Birks, H. J. B., Liu, J., Zhang, S., Jin, L., An, C., Telford, R. J., Cao,
495 X., Wang, Z., Zhang, X., Selvaraj, K., Lu, H., Li, Y., Zheng, Z., Wang, H., Zhou, A., Dong,
496 G., Zhang, J., Huang, X., Bloemendal, J., and Rao, Z.: East Asian summer monsoon
497 precipitation variability since the last deglaciation, *Scientific Reports*, 5, 11186, 2015.

498 Cheng, B., Chen, F., and Zhang, J.: Palaeovegetational and Palaeoenvironmental Changes in
499 Gonghe Basin since Last Deglaciation, *Acta Geographica Sinica*, 11, 1336-1344, 2010 (in
500 Chinese).

501 Cheng, H., Edwards, R. L., Sinha, A., Spötl, C., Yi, L., Chen, S., Kelly, M., Kathayat, G., Wang,
502 X., Li, X., Kong, X., Wang, Y., Ning, Y., and Zhang, H.: The Asian monsoon over the past
503 640,000 years and ice age terminations, *Nature*, 534, 640, 2016.

504 Cheng, Y.: Vegetation and climate change in the north-central part of the Loess Plateau since
505 26,000 years, China University of Geosciences, Master Dissertation, 2011 (in Chinese).

506 Collins, W. J., Bellouin, N., Doutriaux-Boucher, M., Gedney, N., Halloran, P., Hinton, T.,
507 Hughes, J., Jones, C.D., Joshi, M., Liddicoat, S., Martin, G., O'Connor, F., Rae, J., Senior,
508 C., Sitch, S., Totterdell, I., Wiltshire, A., and Woodward, S.: Development and evaluation
509 of an Earth-system model—HadGEM2, *Geoscientific Model Development*, 4, 1051–1075,
510 2011.

511 Cui, M., Luo, Y., and Sun, X.: Paleovegetational and paleoclimatic changed in Ha'ni Lake,
512 Jilin since 5ka BP, *Marine Geology & Quaternary Geology*, 26, 117-122, 2006 (in
513 Chinese).

514 Davis, B. A. S., Brewer, S., Stevenson, A. C., and Guiot, J.: The temperature of Europe during
515 the Holocene reconstructed from pollen data, *Quaternary Science Reviews*, 22, 1701-1716,
516 2003.

517 Dufresne, J.L., Foujols, M.A., Denvil, S., Caubel, A., Marti, O., Aumont, O., Balkanski, Y.,
518 Bekki, S., Bellenger, H., Benschila, R., Bony, S., Bopp, L., Braconnot, P., Brockmann, P.,
519 Cadule, P., Cheruy, F., Codron, F., Cozic, A., Cugnet, D., Noblet, N., Duvel, J.P., Ethe, C.,
520 Fairhead, L., Fichefet, T., Flavoni, S., Friedlingstein, P., Grandpeix, J.Y., Guez, L.,
521 Guilyardi, E., Hauglustaine, D., Hourdin, F., Idelkadi, A., Ghattas, J., Joussaume, S.,
522 Kageyama, M., Krinner, G., Labetoulle, S., Lahellec, A., Lefevre, M.-F., Lefevre, F.,
523 Levy, C., Li, Z.X., Lloyd, J., Lott, F., Madec, G., Mancip, M., Marchand, M., Masson, S.,
524 Meurdesoif, Y., Mignot, J., Musat, I., Parouty, S., Polcher, J., Rio, C., Schulz, M.,
525 Swingedouw, D., Szopa, S., Talandier, C., Terray, P., Viovy, N., and Vuichard, N.:
526 Climate change projections using the IPSL-CM5 Earth system model: from CMIP3 to
527 CMIP5, *Climate Dynamics*, 40, 2123-2165, 2013.

528 Farrera, I., Harrison, S. P., Prentice, I. C., Ramstein, G., Guiot, J., Bartlein, P. J., Bonnefille, R.,
529 Bush, M., Cramer, W., von Grafenstein, U., Holmgren, K., Hooghiemstra, H., Hope, G.,
530 Jolly, D., Lauritzen, S. E., Ono, Y., Pinot, S., Stute, M., and Yu, G.: Tropical climates at the
531 Last Glacial Maximum: a new synthesis of terrestrial palaeoclimate data. I. Vegetation,
532 lake-levels and geochemistry, *Climate Dynamics*, 15, 823-856, 1999.

533 Fischer, N., and Jungclaus, J. H.: Evolution of the seasonal temperature cycle in a transient
534 Holocene simulation: orbital forcing and sea-ice, *Clim. Past*, 7, 1139-1148, 2011.

535 Ganopolski, A., Kubatzki, C., Claussen, M., Brovkin, V., and Petoukhov, V.: The Influence of
536 Vegetation-Atmosphere-Ocean Interaction on Climate During the Mid-Holocene, *Science*,
537 280, 1916-1919, 1998.

538 Gent, P.R., Danabasoglu, G., Donner, L.J., Holland, M.M., Hunke, E.C., Jayne, S.R.,
539 Lawrence, D.M., Neale, R.B., Rasch, P.J., Vertenstein, M., Worley, P.H., Yang, Z., and
540 Zhang, M.: The community climate system model version 4, *Journal of Climate*, 24,
541 4973-4991, 2011.

542 Giorgetta, M.A., Jungclaus, J., Reick, C.H., Legutke, S., Bader, J., Bottinger, M., Brovkin, V.,
543 Crueger, T., Esch, M., Fieg, K., Glushak, K., Gayler, V., Haak, H., Hollweg, H.D., Ilyina,
544 T., Kinne, S., Kornblueh, L., Matei, D., Mauritsen, T., Mikolajewicz, U., Mueller, W.,
545 Notz, D., Pithan, F., Raddatz, T.J., Rast, S., Redler, R., Roeckner, E., Schmidt, H., Schnur,
546 R., Segschneider, J., Six, K.D., Stockhause, M., Timmreck, C., Wegner, J., Widmann, H.,
547 Wieners, K.H., Claussen, M., Marotzke, J., and Stevens, B.: Climate and carbon cycle
548 changes from 1850 to 2100 in MPI-ESM simulations for the Coupled Model
549 Intercomparison Project phase 5, *Journal of Advances in Modeling Earth System*, 5,
550 572-597, 2013.

551 Gong, X.: High-resolution paleovegetation reconstruction from pollen in Jiachuanyuan, Baoji,
552 Capital Normal University, Master Dissertation, 2006 (in Chinese).

553 Guiot, J., and C. Goeury.: PPPBASE, a software for statistical analysis of paleoecological and
554 paleoclimatological data, *Dendrochronologia*, 14, 295-300, 1996.

555 Guiot, J., Torre, F., Jolly, D., Peyron, O., Boreux, J. J., and Cheddadi, R.: Inverse vegetation
556 modeling by Monte Carlo sampling to reconstruct palaeoclimates under changed
557 precipitation seasonality and CO₂ conditions: application to glacial climate in
558 Mediterranean region, *Ecological Modelling*, 127, 119-140, 2000.

559 Guo, L., Feng, Z., Lee, X., Liu, L., and Wang, L.: Holocene climatic and environmental
560 changes recorded in Baahar Nuur Lake in the Ordos Plateau, Southern Mongolia of china,
561 *Chinese Science Bulletin*, 52, 959-966, 2007.

562 Hargreaves, J. C., Annan, J. D., Ohgaito, R., Paul, A., and Abe-Ouchi, A.: Skill and reliability
563 of climate model ensembles at the Last Glacial Maximum and mid-Holocene, *Clim. Past*, 9,
564 811-823, 2013.

565 Harrison, S. P., Bartlein, P. J., Brewer, S., Prentice, I. C., Boyd, M., Hessler, I., Holmgren, K.,
566 Izumi, K., and Willis, K.: Climate model benchmarking with glacial and mid-Holocene
567 climates, *Climate Dynamics*, 43, 671-688, 2014.

568 Harrison, S. P., Bartlein, P. J., K., Izumi, Li, G., Annan, J., Hargreaves, J., Braconnot, P., and
569 Kageyama, M.: Evaluation of CMIP5 paleo-simulations to improve climate projections,
570 *Nature Climate Change*, 5, 735-743, 2015.

571 Harrison, S., P., Braconnot, P., Hewitt, C., and Stouffer, R., J.: Fourth International Workshop
572 of the Palaeoclimate Modelling Intercomparison Project (PMIP): Lauching PMIP2 Phase II,
573 *EOS*, 83, 447-457, 2002.

- 574 Herzsuh, U., Kramer, A., Mischke, S., and Zhang, C.: Quantitative climate and vegetation
575 trends since the late glacial on the northeastern Tibetan Plateau deduced from Koucha
576 Lake pollen spectra, *Quaternary Research*, 71, 162-171, 2009.
- 577 Herzsuh, U., Kürschner, H., and Mischke, S.: Temperature variability and vertical
578 vegetation belt shifts during the last ~50,000 yr in the qilian mountains (ne margin of the
579 tibetan plateau, china), *Quaternary Research*, 66, 133-146, 2006.
- 580 Huang, C., Elis, V. C., and Li, S.: Holocene environmental changes of Western and Northern
581 Qinghai-Xizang Plateau Based on pollen analysis, *Acta Micropalaeontologica Sinica*, 4,
582 423-432, 1996 (in Chinese).
- 583 Jeffrey, S.J., Rotstayn, L.D., Collier, M., Dravitzki, S.M., Hamalainen, C., Moeseneder, C.,
584 Wong, K.K., and Syktus, J.I.: Australia' s CMIP5 submission using the CSIRO-Mk3.6
585 model, *Aust. Meteorol. Oceanogr. J.*, 63, 1-13, 2013.
- 586 Jia, L., and Zhang, Y.: Studies on Palynological assemblages and paleoenvironment of late
587 Quaternary on the east margin of the Chanjiang (Yangtze) river delta, *Acta*
588 *Micropalaeontologica Sinica*, 23, 70-76, 2006 (in Chinese).
- 589 Jiang, D., Lang, X., Tian, Z., and Wang, T.: Considerable Model–Data Mismatch in
590 Temperature over China during the Mid-Holocene: Results of PMIP Simulations, *Journal*
591 *of Climate*, 25, 4135-4153, 2012.
- 592 Jiang, Q., and Piperno., R. D.: Environmental and archaeological implications of a late
593 Quaternary palynological sequence, Poyang lake, Southern China, *Quaternary Research*,
594 52, 250-258, 1999.

595 Jiang, W., Guiot, J., Chu, G., Wu, H., Yuan, B., Hatt é C., and Guo, Z.: An improved
596 methodology of the modern analogues technique for palaeoclimate reconstruction in arid
597 and semi-arid regions, *Boreas*, 39, 145-153, 2010.

598 Jiang, W., Guo, Z., Sun, X., Wu, H., Chu, G., Yuan, B., Hatte, C., and Guiot, J.:
599 Reconstruction of climate and vegetation changes of lake bayanchagan (inner mongolia):
600 holocene variability of the east asian monsoon. *Quaternary Research*, 65, 411-420, 2006.

601 Jiang, W., Leroy, S. G., Ogle, N., Chu, G., Wang, L., and Liu, J.: Natural and authropogenic
602 forest fires recorded in the Holocene pollen record from a Jinchuan peat bog, northeastern
603 China, *Palaeogeography, Palaeoclimatology, Palaeoecology*, 261, 47-57, 2008.

604 Joussaume, S., and Taylor, K. E.: Status of the Paleoclimate Modeling Intercomparison Project,
605 Proc. 1st Int. AMIP Scientific Conf, 425-430, 1995.

606 Joussaume, S., Taylor, K. E., Braconnot, P., Mitchell, J. F. B., Kutzbach, J. E., Harrison, S. P.,
607 Prentice, I. C., Broccoli, A. J., Abe-Ouchi, A., Bartlein, P. J., Bonfils, C., Dong, B., Guiot,
608 J., Herterich, K., Hewitt, C. D., Jolly, D., Kim, J. W., Kislov, A., Kitoh, A., Loutre, M. F.,
609 Masson, V., McAvaney, B., McFarlane, N., de Noblet, N., Peltier, W. R., Peterschmitt, J. Y.,
610 Pollard, D., Rind, D., Royer, J. F., Schlesinger, M. E., Syktus, J., Thompson, S., Valdes, P.,
611 Vettoretti, G., Webb, R. S., Wyputta, U.: Monsoon changes for 6000 years ago: Results of
612 18 simulations from the Paleoclimate Modeling Intercomparison Project (PMIP),
613 *Geophysical Research Letters*, 26, 856-862, 1999.

614 Kaplan, J. O., Bigelow, N. H., Bartlein, P. J., Christensen, T. R., Cramer, W., Harrison, S. P.,
615 Matveyeva, N. V., McGuire, A. D., Murray, D. F., Prentice, I. C., Razzhivin, V. Y., Smith,
616 B., Anderson, P. M., Andreev, A. A., Brubaker, L. B., Edwards, M. E., and Lozhkin, A. V.:
617 Climate change and Arctic ecosystems II: Modeling, palaeodata-model comparisons, and
618 future projections, *Journal of Geophysical Research: Atmospheres*, 108, 2003.

- 619 Kohfeld, K. E. and Harrison, S.: How well we can simulate past climates? Evaluating the
620 models using global palaeoenvironmental datasets, *Quaternary Science Reviews*, 19,
621 321-346, 2000.
- 622 Kong, Z., Xu, Q., Yang, X., Sun, L., Liang, W.: Analysis of sporopollen assemblages of
623 Holocene alluvial deposits in the Yinmahe River Basin, Hebei Province, and preliminary
624 study on temporal and spatial changes of vegetation, *Acta Phytocologica Sinica*, 24, 724,
625 2000 (in Chinese).
- 626 Lee, Y., and Liew, M.: Pollen stratigraphy, vegetation and environment of the last glacial and
627 Holocene-A record from Toushe Basin, central Taiwan,
628 *Palaeogeography, Palaeoclimatology, Palaeoecology*, 287, 58-66, 2010.
- 629 Li, B., and Sun, J.: Vegetation and climate environment during Holocene in Xi'an region of
630 Loess Plateau, China, *Marine Geology and Quaternary Geology*, 3, 125-132, 2005 (in
631 Chinese).
- 632 Li, C., Wu, Y., and Hou, X.: Holocene vegetation and climate in Northeast China revealed
633 from Jingbo Lake sediment, *Quaternary International*, 229, 67-73, 2011.
- 634 Li, L., Lin, P., Yu, Y., Wang, B., Zhou, T., Liu, L., Liu, J., Bao, Q., Xu, S., Huang, W., Xia,
635 K., Pu, Y., Dong, L., Shen, S., Liu, Y., Hu, N., Liu, M., Sun, W., Shi, X., Zheng, W., Wu,
636 B., Song, M., Liu, H., Zhang, X., Wu, G., Xue, W., Huang, X., Yang, G., Song, Z., and
637 Qiao, F.: The flexible global ocean-atmosphere-land system model, Grid-point Version 2:
638 FGOALS-g2, *Adv. Atmos. Sci.*, 30, 543-560, 2013.
- 639 Li, Q., Wu, H., Guo, Z., Yu, Y., Ge, J., Wu, J., Zhao, D., and Sun, A.: Distribution and
640 vegetation reconstruction of the deserts of northern China during the mid-Holocene,
641 *Geophysical Research Letter*, 41, 2184-5191, 2014.

- 642 Li, X., and Liu, J.: Holocene vegetational and environmental changes at Mt. Luoji, Sichuan,
643 *Acta Geographica Sinica*, 1, 44-51, 1988 (in Chinese).
- 644 Li, X., Zhao, K., Dodson, J., and Zhou, X.: Moisture dynamics in central Asia for the last
645 15 kyr: new evidence from Yili Valley, Xinjiang, NW China, *Quaternary Science*
646 *Reviews*, 30, 23-34, 2011.
- 647 Li, X., Zhou, J., and Dodson, J.: The vegetation characteristics of the ‘yuan’ area at yaoxian
648 on the loess plateau in china over the last 12 000 years. *Review of Palaeobotany &*
649 *Palynology*, 124, 1-7, 2003.
- 650 Li, X., Zhou, W., An, Z., and Dodson, J.: The vegetation and monsoon variations at the
651 desert-loess transition belt at Midiwan in northern China for the last 13 ka, *Holocene*, 13,
652 779-784, 2003.
- 653 Li, Z., Hai, Y., Zhou, Y., Luo, R., Zhang, Q.: Pollen Component of Lacustrain Deposit and its
654 Palaeo-environment Significance in the Downstream Region of Urumqi Riever since
655 30Ka BP, *Arid Land Geography*, 24, 201-205, 2001 (in Chinese).
- 656 Liew, M., Huang, Y., and Kuo, M.: Pollen stratigraphy, vegetation and environment of the last
657 glacial and Holocene-A record from Toushe Basin, central Taiwan, *Quaternary*
658 *International*, 14, 16-33, 2006.
- 659 Liu, H., Tang, X., Sun, D., and Wang, K.: Palynofloras of the Dajiuhe Basin in Shennongjia
660 mountains during the last 12.5 ka, *Acta Micropalaeontologica Sinica*, 1, 101-109, 2001 (in
661 Chinese).
- 662 Liu, J., Zhao, S., Cheng, J., Bao, J., and Yin, G.: A study of vegetation and climate evolution
663 since the Holocene near the banks of the Qiangtang River in Hangzhou Bay, *Earth*
664 *Science Frontiers*, 5, 235-245, 2007 (in Chinese).

665 Liu, Y., Liu, J., and Han, J.: Pollen record and climate changing since 12.0ka B. P. in
666 Erlongwan Maar Lake, Jilin province, *Journal of Jilin University (Earth Science Edition)*,
667 39, 93-98, 2009 (in Chinese).

668 Liu, Y., Zhang, S., Liu, J., You, H., and Han, J.: Vegetation and environment history of
669 erlongwan Maar lake during the late Pleistocene on pollen record, *Acta*
670 *Micropalaeontologica Sinica*, 25, 274-280, 2008 (in Chinese).

671 Liu, Z., Harrison, S. P., Kutzbach, J. E., and Otto-Bliesner, B.: Global monsoons in the
672 mid-Holocene and oceanic feedback, *Climate Dynamics*, 22, 157-182, 2004.

673 Liu, Z., Wang, Y., Gallimore, R., Gasse, F., Johnson, T., deMenocal, P., Adkins, J., Notaro, M.,
674 Prentice, I.C., Kutzbach, J., Jacob, R., Behling, P., Wang, L., and Ong, E.: Simulating the
675 transient evolution and abrupt change of Northern Africa atmosphere–ocean–terrestrial
676 ecosystem in the Holocene, *Quaternary Science Reviews*, 26, 1818-1837, 2007.

677 Liu, Z., Zhu, J., Rosenthal, Y., Zhang, X., Otto-Bliesner, B. L., Timmermann, A., Smith, R. S.,
678 Lohmann, G., Zheng, W., and Elison Timm, O.: The Holocene temperature conundrum,
679 *Proceedings of the National Academy of Sciences*, 111, E3501-E3505, 2014.

680 Lu, H., Wu, N., Liu, K.-b., Zhu, L., Yang, X., Yao, T., Wang, L., Li, Q., Liu, X., Shen, C., Li, X.,
681 Tong, G., and Jiang, H.: Modern pollen distributions in Qinghai-Tibetan Plateau and the
682 development of transfer functions for reconstructing Holocene environmental changes,
683 *Quaternary Science Reviews*, 30, 947-966, 2011.

684 Luo, H.: Characteristics of the Holocene sporopollen flora and climate change in the Coq ên
685 area, Tibet, Chengdu University of Technology, Master Dissertation, 2008 (in Chinese).

686 Mann, M. E., Zhang, Z., Hughes, M. K., Bradley, R. S., Miller, S. K., Rutherford, S., and Ni, F.:
687 Proxy-based reconstructions of hemispheric and global surface temperature variations over

688 the past two millennia, *Proceedings of the National Academy of Sciences*, 105,
689 13252-13256, 2008.

690 Marchant, R., Cleef, A., Harrison, S. P., Hooghiemstra, H., Markgraf, V., Van Boxel, J., Ager,
691 T., Almeida, L., Anderson, R., Baied, C., Behling, H., Berrio, J. C., Burbidge, R., Bjorck,
692 S., Byrne, R., Bush, M., Duivenvoorden, J., Flenley, J., De Oliveira, P., Van Gee, B., Graf,
693 K., Gosling, W. D., Harbele, S., Van Der Hammen, T., Hansen, B., Horn, S., Kuhry, P.,
694 Ledru, M. P., Mayle, F., Leyden, B., Lozano-Garcia, S., Melief, A. M., Moreno, P., Moar,
695 N. T., Prieto, A., Van Reenen, G., Salgado-Labouriau, M., Schabitz, F., Schreve-Brinkman,
696 E. J., and Wille, M.: Pollen-based biome reconstructions for Latin America at 0, 6000 and
697 18 000 radiocarbon years ago, *Climate of the Past*, 5, 725-767, 2009.

698 Marcott, S., Shakun, J., U Clark, P., and Mix, A.: A Reconstruction of Regional and Global
699 Temperature for the Past 11,300 Years, *Science*, 1198-1201, 2013.

700 Mauri, A., Davis, B. A. S., Collins, P. M., and Kaplan, J. O.: The climate of Europe during the
701 Holocene: a gridded pollen-based reconstruction and its multi-proxy evaluation,
702 *Quaternary Science Reviews*, 112, 109-127, 2015.

703 Ma, Y., Zhang, H., Pachur, H., Wunnemann, B., Li, J., and Feng, Z.: Late Glacial and
704 Holocene vegetation history and paleoclimate of the Tengger Desert, northwestern China,
705 *Chinese Science Bulletin*, 48, 1457-1463, 2003.

706 Members of the China Quaternary Pollen Data Base.: Pollen-based Biome reconstruction at
707 Middle Holocene (6ka BP) and Last Glacial Maximum (18ka BP) in China, *Acta Botanica*
708 *Sinica*, 42, 1201-1209, 2000.

709 Members, M. P.: Constraints on the magnitude and patterns of ocean cooling at the Last Glacial
710 Maximum, *Nature Geoscience*, 2, 127-130, 2009.

711 Meng, X., Zhu, D., Shao, Z., Han, J., Yu, J., Meng, Q., Lv, R., and Luo, P.: Paleoclimatic and
712 Plaeoenvironmental Evolution Since Holocene in the Ningwu Area, Shanxi Province, *Acta*
713 *Geologica Sinica*, 3, 316-323, 2007 (in Chinese).

714 Ni, J., Sykes, M. T., Prentice, I. C., and Cramer, W.: Modelling the vegetation of China using
715 the process-based equilibrium terrestrial biosphere model BIOME3, *Global Ecology and*
716 *Biogeography*, 9, 463-479, 2000.

717 Oguntunde, P. G., Ajayi, A. E., and Giesen, N.: Tillage and surface moisture effects on
718 bare-soil albedo of a tropical loamy sand, *Soil and Tillage Research*, 85, 107-114, 2006.

719 O'ishi, R., Abe - Ouchi, I. C. Prentice, and S. Sitch.: Vegetation dynamics and plant CO₂
720 responses as positive feedbacks in a greenhouse world, *Geophysical Research Lettters*, v.
721 36, L11706, doi: 10.1029/2009GL038217, 2009.

722 Otto, J., T. Raddatz, M. Claussen, V. Brovkin, and V. Gayler.: Separation of
723 atmosphere-ocean-vegetation feedbacks and synergies for mid-Holocene climate,
724 *Geophysical Research Lettters*, 36, L09701, doi: 10.1029/2009GL037482, 2009.

725 Peyron, O., Guiot, J., Cheddadi, R., Tarasov, P., Reille, M., De Beaulieu, J.L., Bottema, S., and
726 Andrieu, Valerie. : Climatic reconstruction in Europe for 18,000 YR B.P. from pollen data,
727 *Quaternary Research*, 49, 183-196, 1998.

728 Peyron, O., Jolly, D., Bonnefille, R., Vincens, A., and Guiot, J.: Climate of East Africa 6000
729 ¹⁴C Yr B.P. as Inferred from Pollen Data, *Quaternary Research*, 54, 90-101, 2000.

730 Pickett Elizabeth, J., Harrison Sandy, P., Hope, G., Harle, K., Dodson John, R., Peter Kershaw,
731 A., Colin Prentice, I., Backhouse, J., Colhoun Eric, A., D'Costa, D., Flenley, J., Grindrod, J.,
732 Haberle, S., Hassell, C., Kenyon, C., Macphail, M., Martin, H., Martin Anthony, H.,
733 McKenzie, M., Newsome Jane, C., Penny, D., Powell, J., Ian Raine, J., Southern, W.,

734 Stevenson, J., Sutra, J. P., Thomas, I., Kaars, S., and Ward, J.: Pollen-based reconstructions
735 of biome distributions for Australia, Southeast Asia and the Pacific (SEAPAC region) at 0,
736 6000 and 18,000 ¹⁴C yr BP, *Journal of Biogeography*, 31, 1381-1444, 2004.

737 Prentice, I. C., Guiot, J., Huntley, B., Jolly, D., and Cheddadi, R.: Reconstructing biomes from
738 palaeoecological data: A general method and its application to European pollen data at 0
739 and 6 ka, *Climate Dynamics*, 12, 185-194, 1996.

740 Prentice, I. C., and Jolly, D.: Mid-Holocene and glacial-maximum vegetation geography of the
741 northern continents and Africa, *Journal of Biogeography*, 27, 507-519, 2001.

742 Schmidt, G.A., Annan, J.D., Bartlein, P.J., Cook, B.I., Guilyardi, E., Hargreaves, J.C.,
743 Harrison, S.P., Kageyama, M., Legrande, A.N., Konecky, B.L., Lovejoy, S., Mann, M.E.,
744 Masson-Delmotte, V., Risi, C., Thompson, D., Timmermann, A., and Yiou, P.: Using
745 palaeo-climate comparisons to constrain future projections in CMIP5, *Climate of the*
746 *Past*, 10, 221-250, 2014a.

747 Schmidt, G.A., Kelley, M., Nazarenko, L., Ruedy, R., Russell, G.L., Aleinov, I., Bauer, M.,
748 Bauer, S.E., Bhat, M.K., Bleck, R., Canuto, V., Chen, Y., Cheng, Y., Clune, T.L., Del
749 Genio, A., de Fainchtein, R., Faluvegi, G., Hansen, J.E., Healy, R.J., Kiang, N.Y., Koch,
750 D., Lacis, A.A., Legrande, A.N., Lerner, J., Lo, K.K., Matthews, E.E., Menon, S., Miller,
751 R.L., Oinas, V., Oloso, A.O., Perlwitz, J.P., Puma, M.J., Putman, W.M., Rind, D.,
752 Romanou, A., Sato, M., Shindell, D.T., Sun, S., Syed Rahman, A., Tausnev, N., Tsigaridis,
753 K., Under, N., Voulgarakis, A., Yao, M., and Zhang, J.: Configuration and assessment of
754 the GISS ModelE2 contributions to th CMIP5 archive, *Journal of Advances in Modeling*
755 *Earth Systems*, 6, 141-184, 2014b.

756 Shakun, J. D., Clark, P. U., He, F., Marcott, S. A., Mix, A. C., Liu, Z., Otto-Bliesner, B.,
757 Schmittner, A., and Bard, E.: Global warming preceded by increasing carbon dioxide
758 concentrations during the last deglaciation, *Nature*, 484, 49, 2012.

759 Shen, C., Liu, K., Tang, L., Overpeck, J. T.: Quantitative relationships between modern
760 pollen rain and climate in the Tibetan Plateau, *Review of Palaeobotany and Palynology*,
761 140, 61-77, 2006.

762 Shen, J., Jones, R. T., Yang, X., Dearing, J. A., and Wang, S.: The holocene vegetation
763 history of lake Erhai, Yunnan Province, southwestern China: the role of climate and human
764 forcings, *Holocene*, 16, 265-276, 2006.

765 Shen, J., Liu, X., Matsumoto, R., Wang, S., Yang, X., Tang, L., and Shen, C.: Multi-index
766 high-resolution paleoclimatic evolution of sediments in Qinghai Lake since the late glacial
767 period, *Science in China Series D: Earth Sciences*, 6, 582-589, 2004 (in Chinese).

768 Shu, J., Wang, W., and Chen, Y.: Holocene vegetation and environment changes in the NW
769 Taihu Plain, Jiangsu Province, East China, *Acta Micropalaeontologica Sinica*, 2, 210-221,
770 2007 (in Chinese).

771 Shu, Q., Xiao, J., Zhang, M., Zhao, Z., Chen, Y., and Li, J.: Climate Change in Northern
772 Jiangsu Basin since the Last Interglacial: *Geological Science and Technology Information*,
773 5, 59-64, 2008 (in Chinese).

774 Sun, A., and Feng, Z.: Holocene climate reconstructions from the fossil pollen record at Qigai
775 nuur in the southern Mongolian Plateau, *The Holocene*, 23, 1391-1402, 2013.

776 Sun, L., Xu, Q., Yang, X., Liang, W., Sun, Z., and Chen, S.: Vegetation and environmental
777 changes in the Xuanhua Basin of Hebei Province since Postglacial, *Journal of*
778 *Geomechanics*, 4, 303-308, 2001 (in Chinese).

779 Sun, Q., Zhou, J., Shen, J., Cheng, P., Wu, F., and Xie, X.: Mid-Holocene environmental
780 characteristics recorded in the sediments of the Bohai Sea in the northern environmental
781 sensitive zone, *Science in China (Series D)*, 9, 838-849, 2006 (in Chinese).

782 Sun, X., and Xia, Z.: Paleoenvironment Changes Since Mid-Holocene Revealed by a
783 Palynological Sequence from Sihenan Profile in Luoyang, Henan Province, *Acta*
784 *Scientiarum Naturalium Universitatis Pekinensis*, 2, 289-294, 2005 (in Chinese).

785 Sun, X., Wang, F., and Sun, C.: Pollen-climate response surfaces of selected taxa from
786 Northern China, *Science in China Series D-Earth Sciences*, 39, 486, 1996.

787 Swann, A. L., Fung, I. Y., Levis, S., Bonan, G. B., and Doney, S. C.: Changes in Arctic
788 vegetation amplify high-latitude warming through the greenhouse effect, *Proceedings of*
789 *the National Academy of Sciences*, 107, 1295-1300, 2010.

790 Sykes, M.T., Prentice, I.C., and Laarif, F.: Quantifying the impact of global climate change on
791 potential natural vegetation, *Climatic Change*, 41, 37-52, 1999.

792 Tang, L., and An, C.: Holocene vegetation change and pollen record of drought events in the
793 Loess Plateau, *Progress in Natural Science*, 10, 1371-1382, 2007 (in Chinese).

794 Tang, L., and Shen, C.: Holocene pollen records of the Qinghai-Xizang Plateau, *Acta*
795 *Micropalaeontologica Sinica*, 4, 407-422, 1996 (in Chinese).

796 Tang, L., Shen, C., Kong, Z., Wang, F., and Liao, K.: Pollen evidence of climate during the
797 last glacial maximum in Eastern Tibetan Plateau, *Journal of Glaciology*, 2, 37-44, 1998
798 (in Chinese).

799 Tao, S., An, C., Chen, F., Tang, L., Wang, Z., Lv, Y., Li, Z., Zheng, T., and Zhao, J.:
800 Vegetation and environment since the 16.7cal ka B.P. in Balikun Lake, Xinjiang, China,
801 *Chinese Science Bulletin*, 11, 1026-1035, 2010 (in Chinese).

802 Taylor, K.E., Crucifix, M., Braconnot, P., Hewitt, C. D., Doutriaux. C., Broccoli, A. J., Mitchell,
803 J. F. B., Webb, M. J.: Estimating shortwave radiative forcing and response in climate
804 models, *J. Clim*, 20, 2530-2543, 2007.

805 Voldoire, A., Sanchez-Gomez, E., Salas y Melia, D., Decharme, B., Cassou, C., Senesi, S.,
806 Valcke, S., Beau, I., Alias, A., Chevallier, M., Deque, M., Deshayes, J., Douville, H.,
807 Fernandez, E., Madec, G., Maisonnave, E., Moine, M., Planton, S., Saint-Martin, D.,
808 Szopa, S., Tyteca, S., Alkama, R., Belamari, S., Braun, A., Coquart, L., and Chauvin, F.:
809 The CNRM-CM5.1 global climate model: description and basic evaluation, *Climate*
810 *Dynamics*, 40, 2091-2121, 2012.

811 Wang, H., Liu, H., Zhu, J., and Yin, Y.: Holocene environmental changes as recorded by
812 mineral magnetism of sediments from Anguli-nuur Lake, southeastern Inner Mongolia
813 Plateau, China, *Palaeogeography, Palaeoclimatology, Palaeoecology*, 285, 30-49, 2010.

814 Wang, H., Liu, H., Zhu, J., and Yin, Y.: Holocene environmental changes as recorded by
815 mineral magnetism of sediments from Anguli-nuur Lake, southeastern Inner Mongolia
816 Plateau, China, *Palaeogeography, Palaeoclimatology, Palaeoecology*, 285, 30-49, 2010.

817 Wang, S., Lv, H., and Liu, J.: Environmental characteristics of the early Holocene suitable
818 period revealed by the high-resolution sporopollen record of Huguangyan Lake, Chinese
819 *Science Bulletin*, 11, 1285-1291, 2007 (in Chinese).

820 Wang, X., Wang, J., Cao, L., Yang, J., Yang, X., Peng, Z., and Jin, G.: Late Quaternary
821 Pollen Records and Climate Significance in Guangzhou, *Acta Scientiarum Naturalium*
822 *Universitatis Sunyatseni*, 3, 113-121, 2010 (in Chinese).

823 Wang, X., Zhang, G., Li, W., Zhang, X., Zhang, E., and Xiao, X.: Environmental changes
824 during early-middle holocene from the sediment record of the chaohu lake, anhui province,
825 *Chinese Science Bulletin*, 53, 153-160, 2008.

826 Wang, X., Zhang, G., Li, W., Zhang, X., Zhang, E., and Xiao, X.: Environmental changes
827 during early-middle holocene from the sediment record of the chaohu lake, anhui province,
828 Chinese Science Bulletin, 53, 153-160, 2008.

829 Wang, Y., Wang, S., Jiang, F., and Tong, G.: Palynological records in Xipu section,
830 Yangyuan, Journal of Geomechanics, 2, 171-175, 2003 (in Chinese).

831 Wang, Y., Wang, S., Zhao, Z., Qin, Y., Ma, Y., Sun, J., Sun, H., and Tian, M.: Vegetation and
832 Environmental Changes in Hexiqten Qi of Inner Mongolia in the Past 16000 Years, Acta
833 Geoscientica Sinica, 5, 449-453, 2005 (in Chinese).

834 Wang, Y., Zhao, Z., Qiao, Y., Wang, S., Li, C., and Song, L.: Paleoclimatic and
835 paleoenvironmental evolution since the late glacial epoch as recorded by sporopollen from
836 the Hongyuan peat section on the Zoigê Plateau, northern Sichuan, China, Geological
837 Bulletin of China, 7, 827-832, 2006 (in Chinese).

838 Watanabe, S., Hajima, T., Sudo, K., Nagashima, T., Takemura, T., Okajima, H., Nozawa, T.,
839 Kawase, H., Abe, M., Yokohata, T., Ise, T., Sato, H., Kato, E., Takata, K., Emori, S., and
840 Kawamiya, M.: MIROC-ESM 2010: model description and basic results of
841 CMIP5-20c3m experiments, Geoscientific Model Development, 4, 845-872, 2011.

842 Webb, T. III.: Global paleoclimatic data base for 6000 yr BP, Brown Univ., Providence, RI
843 (USA). Dept. of Geological Sciences, DOE/EV/10097-6; Other: ON: DE85006628 United
844 States Other: ON: DE85006628 NTIS, PC A08/MF A01. HEDB English, 1985.

845 Wen, R., Xiao, J., Chang, Z., Zhai, D., Xu, Q., Li, Y. and Itoh, S.: Holocene precipitation and
846 temperature variations in the East Asian monsoonal margin from pollen data from Hulun
847 Lake in northeastern Inner Mongolia, China, Boreas, 39, 262-272, 2010.

848 Wen, R., Xiao, J., Chang, Z., Zhai, D., Xu, Q., Li, Y. and Itoh, S.: Holocene precipitation and
849 temperature variations in the East Asian monsoonal margin from pollen data from Hulun
850 Lake in northeastern Inner Mongolia, China, *Boreas*, 39, 262-272, 2010.

851 Wischniewski, J., Mischke, S., Wang, Y., and Herzschuh, U.: Reconstructing climate
852 variability on the northeastern Tibetan Plateau since the last Lateglacial – a multi-proxy,
853 dual-site approach comparing terrestrial and aquatic signals, *Quaternary Science Reviews*,
854 30, 82-97, 2011.

855 Wischniewski, J., Mischke, S., Wang, Y., and Herzschuh, U.: Reconstructing climate
856 variability on the northeastern Tibetan Plateau since the last Lateglacial – a multi-proxy,
857 dual-site approach comparing terrestrial and aquatic signals, *Quaternary Science Reviews*,
858 30, 82-97, 2011.

859 Wohlfahrt, J., Harrison, S. P., and Braconnot, P.: Synergistic feedbacks between ocean and
860 vegetation on mid- and high-latitude climates during the mid-Holocene, *Climate Dynamics*,
861 22, 223-238, 2004.

862 Wu, H., Guiot, J., Brewer, S., and Guo, Z.: Climatic changes in Eurasia and Africa at the last
863 glacial maximum and mid-Holocene: reconstruction from pollen data using inverse
864 vegetation modeling, *Climate Dynamics*, 29, 211-229, 2007.

865 Wu, H., Luo, Y., Jiang, W., Li, Q., Sun, A., and Guo, Z.: Paleoclimate reconstruction from
866 pollen data using inverse vegetation approach: Validation of model using modern data, 36,
867 520-529 (in Chinese), 2016.

868 Wu, H., Ma, Y., Feng, Z., Sun, A., Zhang, C., Li, F., and Kuang, J.: A high resolution record
869 of vegetation and environmental variation through the last ~25,000 years in the western
870 part of the Chinese Loess Plateau, *Palaeogeography, Palaeoclimatology, Palaeoecology*,
871 273, 191-199, 2009.

- 872 Xia, Y.: Preliminary study on vegetational development and climatic changes in the Sanjiang
873 Plain in the last 12000 years, *Scientia Geographica Sinica*, 8, 241-249, 1988 (in Chinese).
- 874 Xia, Z., Chen, G., Zheng, G., Chen, F., and Han, J.: Climate background of the evolution from
875 Paleolithic to Neolithic cultural transition during the last deglaciation in the middle
876 reaches of the Yellow River, *Chinese Science Bulletin*, 47, 71-75, 2002.
- 877 Xiao, J., Lv, H., Zhou, W., Zhao, Z., and Hao, R.: Pollen Vegetation and Environmental
878 Evolution of the Great Lakes in Jiangxi Province since the Last Glacial Maximum,
879 *Science in China (Series D)*, 6, 789-797, 2007 (in Chinese).
- 880 Xiao, J., Xu, Q., Nakamura, T., Yang, X., Liang, W., and Inouchi, Y.: Holocene vegetation
881 variation in the Daihai Lake region of north-central China: a direct indication of the Asian
882 monsoon climatic history, *Quaternary Science Reviews*, 23, 1669-1679, 2004.
- 883 Xiao, X., Haberle, S. G., Shen, J., Yang, X., Han, Y., Zhang, E., and Wang, S.: Latest
884 Pleistocene and Holocene vegetation and climate history inferred from an alpine
885 lacustrine record, northwestern Yunnan Province, southwestern China, *Quaternary
886 Science reviews*, 86, 35-48, 2014.
- 887 Xie, Y., Li, C., Wang, Q., and Yin, H.: Climatic Change Since 9 ka B. P.: Evidence from
888 Jiangling Area, Jiangnan Plain, China, *Scientia Geographica Sinica*, 2, 199-204, 2006 (in
889 Chinese).
- 890 Xin, X., Wu, T., and Zhang, J.: Introduction of CMIP5 experiments carried out with the
891 climate system models of Beijing climate Center, *Adv. Clim. Change. Res.*, 4, 41-49,
892 2013.
- 893 Xu, J.: Analysis of the Holocene Loess Pollen in Xifeng Area and its Vegetation Evolution,
894 Capital Normal University, Master Dissertation, 2006 (in Chinese).

- 895 Xu, Q., Chen, S., Kong, Z., and Du, N.: Preliminary discussion of vegetation succession and
896 climate change since the Holocene in the Baiyangdian Lake district, *Acta Phytoecologica*
897 and *Geobotanica Sinica*, 2, 65-73, 1988 (in Chinese).
- 898 Xu, Q., Yang, Z., Cui, Z., Yang, X., and Liang.: A Study on Pollen Analysis of Qiguoshan
899 Section and Ancestor Living Environment in Chifeng Area, Nei Mongol, *Scientia*
900 *Geographica Sinica*, 4, 453-456, 2002 (in Chinese).
- 901 Xu, Y.: The assemblage of Holocene spore pollen and its environment in Bosten Lake area
902 Xinjiang, *Arid land Geography*, 2, 43-49, 1998 (in Chinese).
- 903 Xue, S., and Li, X.: Holocene vegetation characteristics of the southern loess plateau in the
904 weihe river valley in china, *Review of Palaeobotany & Palynology*, 160 46-52, 2010.
- 905 Yang, J., Cui, Z., Yi, Zhao., Zhang, W., and Liu, K.: Glacial Lacustrine Sediment's Response
906 to Climate Change since Holocene in Diancang Mountain, *Acta Geographica Sinica*, 4,
907 525-533, 2004 (in Chinese).
- 908 Yang, X., Wang, S., and Tong, G.: Character of a nology and changes of monsoon climate
909 over the last 10000 years in Gucheng Lake, Jiangsu province, *Journal of Integrative Plant*
910 *Biology*, 7, 576-581, 1996 (in Chinese).
- 911 Yang, Y., and Wang, S.: Study on mire development and paleoenvironment change since
912 8.0ka B.P. in the northern part of the Sangjiang Plain, *Scientia Geographica Sinica*, 23,
913 32-38, 2003 (in Chinese).
- 914 Yang, Z.: Reconstruction of climate and environment since the Holocene in Diaojaohaizi
915 Lake Area, Daqing Mountains, Inner Mongolia, *Acta Ecologica Sinica*, 4, 538-543, 2001
916 (in Chinese).

- 917 Yu, L., Wang, N., Cheng, H., Long, H., and Zhao, Q.: Holocene environmental change in the
918 marginal area of the asian monsoon: a record from Zhuye lake, nw china, *Boreas*, 38,
919 349-361, 2009.
- 920 Yukimoto, S., Adachi, Y., Hosaka, M., Sakami, T., Yoshimura, H., Hirabara, M., Tanaka,
921 T.Y., Shindo, E., Tsujino, H., Deushi, M., Mizuta, R., Yabu, S., Obata, A., Nakano, H.,
922 Koshiro, T., Ose, T., and Kitoh, A.: A new global climate model of the meteorological
923 research institute: MRI-CGCM3-model description and basic performance, *Journal of the*
924 *Meteorological Society of Japan*, 90A, 23-64, 2012.
- 925 Zhang, W., Mu, K., Cui, Z., Feng, J., and Yang, J.: Record of the environmental change since
926 Holocene in the region of Gongwang mountain, Yunan Province, *Earth and Environment*,
927 4, 343-350, 2007 (in Chinese).
- 928 Zhang, Y. G., Pagani, M., and Liu, Z.: A 12-Million-Year Temperature History of the tropical
929 Pacific Ocean, *Science*, 344, 84-87, 2014.
- 930 Zhang, Y., and Yu, S.: Palynological assemblages of late Quaternary from the Shenzhen
931 region and its paleoenvironment evolution, 2, 109-114, 1999 (in Chinese).
- 932 Zhang, Y., Jia, L., and Lyu, B.: Studies on Evolution of Vegetation and Climate since 7000
933 Years ago in Estuary of Changjiang River Region, *Marine Science Bulletin*, 3, 27-34,
934 2004 (in Chinese).
- 935 Zhang, Y., Song, M., and Welker, J. M.: Simulating Alpine Tundra Vegetation Dynamics in
936 Response to Global Warming in China, *Global Warming*, Stuart Arthur Harris (Ed.),
937 ISBN: 978-953-307-149-7, InTech, 11, 221-250, 2010.
- 938 Zhang, Z., Xu, Q., Li, Y., Yang, X., Jin, Z., and Tang, J.: Environmental changes of the Yin
939 ruins area based on pollen analysis, *Quaternary Science*, 27, 461-468, 2007 (in Chinese).

940 Zhao, J., Hou, Y., Du, J., and Chen, Y.: Holocene environmental changes in the Guanzhong
941 Plain, 1, 17-22, 2003 (in Chinese).

942 Zhao, Y., Yu, Z., Chen, F., Ito, E., and Zhao, C.: Holocene vegetation and climate history at
943 Hurleg Lake in the Qaidam Basin, northwest China, *Review of Palaeobotany and*
944 *palynology*, 145, 275-288, 2007.

945 Zheng, R., Xu, X., Zhu, J., Ji, F., Huang, Z., Li, J.: Division of late Quaternary strata and
946 analysis of palaeoenvironment in Fuzhou Basin, *Seismology and Geology*, 4, 503-513,
947 2002 (in Chinese).

948 Zheng, X., Zhang, H., Ming, Q., Chang, F., Meng, H., Zhang, W., Liu, M., Shen, C.:
949 Vegetational and environmental changes since 15ka B.P. recorded by lake Lugu in the
950 southwest monsoon domain region, 6, 1314-1326, 2014 (in Chinese).

951 Zhou, J., Liu, D., Zhuang, Z., Wang, Z., and Liu, L.: The sediment layers and the records of
952 the Palaeoenvironment in the Chaoyanggang Lagoon, Rongcheng City of Shandong
953 Province Since Holocene Transgression, *Periodical of Ocean University of China*, 38,
954 803-808, 2008 (in Chinese).

955 Zhu, C., Ma, C., Zhang, W., Zheng, C., Tan, L., Lu, X., Liu, K., and Chen, H.: Pollen record
956 from Dajiuhu Basin of Shennongjia and environmental changes since 15.753ka B.P.,
957 *Quaternary Sciences*, 5, 814-826, 2006 (in Chinese).

958 Zou, S., Cheng, G., Xiao, H., Xu, B., and Feng, Z.: Holocene natural rhythms of vegetation
959 and present potential ecology in the western Chinese loess plateau, *Quaternary*
960 *International*, 194, 55-67, 2009.

961

962

Table 1. Basic information of the pollen dataset used in this study

Site	Lat	Lon	Alt	Webb 1-7	Source
Sujiawan	35.54	104.52	1700	2	original data (Zou et al., 2009)
Xiaogou	36.10	104.90	1750	2	original data (Wu et al., 2009)
Dadiwan	35.01	105.91	1400	1	original data (Zou et al., 2009)
Sanjiaocheng	39.01	103.34	1320	1	Chen et al., 2006
Chadianpo	36.10	114.40	65	2	Zhang et al., 2007
Qindeli	48.08	133.25	60	2	Yang and Wang, 2003
Fuyuanchuangye	47.35	133.03	56	3	Xia, 1988
Jingbo Lake	43.83	128.50	350	2	Li et al., 2011
Hani Lake	42.22	126.52	900	1	Cui et al., 2006
Jinchuan	42.37	126.43	662	5	Jiang et al., 2008
Maar Lake	42.30	126.37	724	1	Liu et al., 2009
Maar Lake	42.30	126.37	724	1	Liu et al., 2008
Xie Lake SO4	37.38	122.52	0	1	Zhou et al., 2008
Nanhuiheming Core	31.05	121.58	7	2	Jia and Zhang, 2006
Toushe	23.82	120.88	650	1	Liu et al., 2006
Dongyuan Lake	22.17	120.83	415	2	Lee et al., 2010
Yonglong CY	31.78	120.44	5	3	Zhang et al., 2004
Hangzhou HZ3	30.30	120.33	6	4	Liu et al., 2007
Xinhua XH1	32.93	119.83	2	3	Shu et al., 2008
ZK01	31.77	119.80	6	2	Shu et al., 2007
Chifeng	43.97	119.37	503	2	Xu et al., 2002
SZK1	26.08	119.31	9	1	Zheng et al., 2002
Gucheng	31.28	118.90	6	4	Yang et al., 1996
Lulong	39.87	118.87	23	2	Kong et al., 2000
Hulun Lake	48.92	117.42	545	1	Wen et al., 2010
CH-1	31.56	117.39	5	2	Wang et al., 2008
Sanyi profile	43.62	117.38	1598	4	Wang et al., 2005
Xiaoniuchang	42.62	116.82	1411	1	Liu et al., 2002
Haoluku	42.87	116.76	1333	2	Liu et al., 2002
Liuzhouwan	42.71	116.68	1410	7	Liu et al., 2002
Poyang Lake 103B	28.87	116.25	16	4	Jiang and Piperno, 1999
Baiyangdian	38.92	115.84	8	2	Xu et al., 1988
Bayanchagan	42.08	115.35	1355	1	Jiang et al., 2006
Huangjiapu	40.57	115.15	614	7	Sun et al., 2001
Dingnan	24.68	115.00	250	2	Xiao et al., 2007
Guang1	36.02	114.53	56	1	Zhang et al., 2007
Angulinao	41.33	114.35	1315	1	Liu et al., 2010
Yangyuanxipu	40.12	114.22	921	6	Wang et al., 2003

Shenzhen Sx07	22.75	113.78	2	2	Zhang and Yu, 1999
GZ-2	22.71	113.51	1	7	Wang et al., 2010
Daihai99a	40.55	112.66	1221	2	Xiao et al., 2004
Daihai	40.55	112.66	1221	2	Sun et al., 2006
Sihenan profile	34.80	112.40	251	1	Sun and Xia, 2005
Diaojiaohaizi	41.30	112.35	2015	1	Yang et al., 2001
Ganhaizi	39.00	112.30	1854	3	Meng et al., 2007
Jiangling profile	30.35	112.18	37	1	Xie et al., 2006
Helingeer	40.38	111.82	1162	3	Li et al., 2011
Shennongjia2	31.75	110.67	1700	1	Liu et al., 2001
Huguangyan Maar Lake B	21.15	110.28	59	2	Wang et al., 2007
Yaoxian	35.93	110.17	1556	2	Li et al., 2003
Jixian	36.00	110.06	1005	6	Xia et al., 2002
Shennongjia Dajiu Lake	31.49	110.00	1760	2	Zhu et al., 2006
Qigai nuur	39.50	109.85	1300	1	Sun and Feng, 2013
Beizhuangcun	34.35	109.53	519	1	Xue et al., 2010
Lantian	34.15	109.33	523	1	Li and Sun, 2005
Bahanniao	39.32	109.27	1278	1	Guo et al., 2007
Midiwan	37.65	108.62	1400	1	Li et al., 2003
Jinbian	37.50	108.33	1688	2	Cheng, 2011
Xindian	34.38	107.80	608	1	Xue et al., 2010
Nanguanzhuang	34.43	107.75	702	1	Zhao et al., 2003
Xifeng	35.65	107.68	1400	3	Xu, 2006
Jiyuan	37.13	107.40	1765	3	Li et al., 2011
Jiacunyuan	34.27	106.97	1497	2	Gong, 2006
Dadiwan	35.01	105.91	1400	1	Zou et al., 2009
Maying	35.34	104.99	1800	1	Tang and An, 2007
Huiningxiaogou	36.10	104.90	1750	2	Wu et al., 2009
Sujiawan	35.54	104.52	1700	2	Zou et al., 2009
QTH02	39.07	103.61	1302	1	Li et al., 2009
Laotanfang	26.10	103.20	3579	2	Zhang et al., 2007
Hongshui River2	38.17	102.76	1511	1	Ma et al., 2003,
Ruoergai	33.77	102.55	3480	1	Cai, 2006
Hongyuan	32.78	102.52	3500	2	Wang et al., 2006
Dahaizi	27.50	102.33	3660	1	Li et al., 1988
Shayema Lake	28.58	102.22	2453	1	Tang and Shen, 1996
Luanhaizi	37.59	101.35	3200	5	Herzschuh et al., 2006
Lugu Lake	27.68	100.80	2692	1	Zheng et al., 2014
Qinghai Lake	36.93	100.73	3200	2	Shen et al., 2004
Dalianhai	36.25	100.41	2850	3	Cheng et al., 2010
Erhai ES Core	25.78	100.19	1974	1	Shen et al., 2006
Xianmachi profile	25.97	99.87	3820	7	Yang et al., 2004

TCK1	26.63	99.72	3898	1	Xiao et al., 2014
Yidun Lake	30.30	99.55	4470	4	Shen et al., 2006
Kuhai lake	35.30	99.20	4150	1	Wischniewski et al., 2011
Koucha lake	34.00	97.20	4540	2	Herzschuh et al., 2009
Hurleg	37.28	96.90	2817	2	Zhao et al., 2007
Basu	30.72	96.67	4450	3	Tang et al., 1998
Tuolekule	43.34	94.21	1890	1	An et al., 2011
Balikun	43.62	92.77	1575	1	Tao et al., 2010
Cuona	31.47	91.51	4515	3	Tang et al., 2009
Dongdaohaizi2	44.64	87.58	402	1	Li et al., 2001
Bositeng Lake	41.96	87.21	1050	1	Xu, 1998
Cuoqin	31.00	85.00	4648	4	Luo, 2008
Yili	43.86	81.97	928	2	Li et al., 2011
Bangong Lake	33.75	78.67	4241	1	Huang et al., 1996
Shengli	47.53	133.87	52	2	CQPD, 2000
Qingdeli	48.05	133.17	52	1	CQPD, 2000
Changbaishan	42.22	126.00	500	2	CQPD, 2000
Liuhe	42.90	125.75	910	7	CQPD, 2000
Shuangyang	43.27	125.75	215	1	CQPD, 2000
Xiaonan	43.33	125.33	209	1	CQPD, 2000
Tailai	46.40	123.43	146	5	CQPD, 2000
Sheli	45.23	123.31	150	4	CQPD, 2000
Tongtu	45.23	123.30	150	7	CQPD, 2000
Yueyawan	37.98	120.71	5	1	CQPD, 2000
Beiwangxu	37.75	120.61	6	1	CQPD, 2000
East Tai Lake1	31.30	120.60	3	1	CQPD, 2000
Suzhou	31.30	120.60	2	7	CQPD, 2000
Sun-Moon Lake	23.51	120.54	726	2	CQPD, 2000
West Tai Lake	31.30	119.80	1	1	CQPD, 2000
Changzhou	31.43	119.41	5	1	CQPD, 2000
Dazeyin	39.50	119.17	50	7	CQPD, 2000
Hailaer	49.17	119.00	760	2	CQPD, 2000
Cangumiao	39.97	118.60	70	1	CQPD, 2000
Qianhuzhuang	40.00	118.58	80	6	CQPD, 2000
Reshuitang	43.75	117.65	1200	1	CQPD, 2000
Yangerzhuang	38.20	117.30	5	7	CQPD, 2000
Mengcun	38.00	117.06	7	5	CQPD, 2000
Hanjiang-CH2	23.48	116.80	5	2	CQPD, 2000
Hanjiang-SH6	23.42	116.68	3	7	CQPD, 2000
Hanjiang-SH5	23.45	116.67	8	2	CQPD, 2000
Hulun Lake	48.90	116.50	650	1	CQPD, 2000
Heitutang	40.38	113.74	1060	1	CQPD, 2000
Zhujiang delta PK16	22.73	113.72	15	7	CQPD, 2000

Angulitun	41.30	113.70	1400	7	CQPD, 2000
Bataigou	40.92	113.63	1357	1	CQPD, 2000
Dahewan	40.87	113.57	1298	2	CQPD, 2000
Yutubao	40.75	112.67	1254	7	CQPD, 2000
Zhujiang delta K5	22.78	112.63	12	1	CQPD, 2000
Da-7	40.52	112.62	1200	3	CQPD, 2000
Hahai-1	40.17	112.50	1200	5	CQPD, 2000
Wajianggou	40.50	112.50	1476	4	CQPD, 2000
Shuidong Core A1	21.75	111.07	-8	2	CQPD, 2000
Dajahu	31.50	110.33	1700	2	CQPD, 2000
Tianshuigou	34.87	109.73	360	7	CQPD, 2000
Mengjiawan	38.60	109.67	1190	7	CQPD, 2000
Fuping BK13	34.70	109.25	422	7	CQPD, 2000
Yaocun	34.70	109.22	405	2	CQPD, 2000
Jinbian	37.80	108.60	1400	4	CQPD, 2000
Dishaogou	37.83	108.45	1200	2	CQPD, 2000
Shuidonggou	38.20	106.57	1200	5	CQPD, 2000
Jiuzhoutai	35.90	104.80	2136	7	CQPD, 2000
Luojishan	27.50	102.40	3800	1	CQPD, 2000
RM-F	33.08	102.35	3400	2	CQPD, 2000
Hongyuan	33.25	101.57	3492	1	CQPD, 2000
Wasong	33.20	101.52	3490	1	CQPD, 2000
Guhu Core 28	27.67	100.83	2780	7	CQPD, 2000
Napahai Core 34	27.80	99.60	3260	2	CQPD, 2000
Lop Nur	40.50	90.25	780	7	CQPD, 2000
Chaiwobao1	43.55	87.78	1100	2	CQPD, 2000
Chaiwobao2	43.33	87.47	1114	1	CQPD, 2000
Manasi	45.97	84.83	257	2	CQPD, 2000
Wuqia	43.20	83.50	1000	7	CQPD, 2000
Madagou	37.00	80.70	1370	2	CQPD, 2000
Tongyu	44.83	123.10	148	5	CQPD, 2000
Nanjing	32.15	119.05	10	2	CQPD, 2000
Banpo	34.27	109.03	395	1	CQPD, 2000
QL-1	34.00	107.58	2200	7	CQPD, 2000
Dalainu	43.20	116.60	1290	7	CQPD, 2000
Qinghai	36.55	99.60	3196	2	CQPD, 2000

964

965

966

967

968

969 **Table 2. Earth's orbital parameters and trace gases as recommended by the PMIP3**
 970 **project**

Simulation	Orbital parameters			Trace gases		
	Eccentricity	Obliquity(°)	Angular precession(°)	CO ₂ (ppmv)	CH ₄ (ppbv)	N ₂ O(ppbv)
PI	0,0167724	23,446	102,04	280	760	270
MH	0,018682	24,105	0,87	280	650	270

971

972

973 **Table 3. PMIP3 model characteristics and references**

<i>Model Name</i>	<i>Modelling centre</i>	<i>Type</i>	<i>Grid</i>	<i>Reference</i>
BCC-CSM-1-1	BCC-CMA (China)	AOVGCM	Atm: 128 × 64 × L26; Ocean: 360 × 232 × L40	Xin et al. (2013)
CCSM4	NCAR (USA)	AOGCM	Atm: 288 × 192 × L26; Ocean: 320 × 384 × L60	Gent et al. (2011)
CNRM-CM5	CNRM&CERFACS (France)	AOGCM	Atm: 256 × 128 × L31; Ocean: 362 × 292 × L42	Voltaire et al. (2012)
CSIRO-Mk3-6-0	QCCCE, Australia	AOGCM	Atm: 192 × 96 × L18; Ocean: 192 × 192 × L31	Jeffrey et al. (2013)
FGOALS-g2	LASG-IAP (China)	AOVGCM	Atm: 128 × 60 × L26; Ocean: 360 × 180 × L30	Li et al. (2013)
FGOALS-s2	LASG-IAP (China)	AOVGCM	Atm: 128 × 108 × L26; Ocean: 360 × 180 × L30	Bao et al. (2013)
GISS-E2-R	GISS (USA)	AOGCM	Atm: 144 × 90 × L40; Ocean: 288 × 180 × L32	Schmidt et al. (2014a,b)
HadGEM2-CC	Hadley Centre (UK)	AOVGCM	Atm: 192 × 145 × L60; Ocean: 360 × 216 × L40	Collins et al. (2011)
HadGEM2-ES	Hadley Centre (UK)	AOVGCM	Atm: 192 × 145 × L38; Ocean: 360 × 216 × L40	Collins et al. (2011)
IPSL-CM5A-LR	IPSL (France)	AOVGCM	Atm: 96 × 96 × L39; Ocean: 182 × 149 × L31	Dufresne et al. (2013)
MIROC-ESM	Utokyo&NIES (Japan)	AOVGCM	Atm: 128 × 64 × L80; Ocean: 256 × 192 × L44	Watanabe et al. (2011)
MPI-ESM-P	MPI (Germany)	AOGCM	Atm: 196 × 98 × L47; Ocean: 256 × 220 × L40	Giorgetta et al. (2013)
MRI-CGCM3	MRI (Japan)	AOGCM	Atm: 320 × 160 × L48; Ocean: 364 × 368 × L51	Yukimoto et al. (2012)

974

975

976

977 **Table 4. Important values for each plant life form used in the ΔV statistical calculation**
 978 **as assigned to the megabiomes**

<i>Megabiomes</i>	<i>Life form</i>		
	Trees	Grass/grass	Bare ground
<i>Tropical forest</i>	1		
<i>Warm mixed forest</i>	1		
<i>Temperate forest</i>	1		
<i>Boreal forest</i>	1		
<i>Grassland and dry shrubland</i>	0.25	0.75	
<i>Savanna and dry woodland</i>	0.5	0.5	
<i>Desert</i>		0.25	0.75
<i>Tundra</i>		0.75	0.25

979

980 **Table 5. Attribute values and the weights for plant life forms used by the ΔV statistic**

<i>Life form</i>	<i>Attribute</i>			
Trees	Evergreen	Needle-leaf	Tropical	Boreal
<i>Tropical forest</i>	1	0	1	0
<i>Warm mixed forest</i>	0.75	0.25	0	0
<i>Temperate forest</i>	0.5	0.5	0	0.5
<i>Boreal forest</i>	0.25	0.75	0	1
<i>Grassland and dry shrubland</i>	0.75	0.25	0.75	0
<i>Savanna and dry woodland</i>	0.25	0.75	0	0.5
<i>weights</i>	0.2	0.2	0.3	0.3
Grass/Shrub	Warm	Arctic/alpine		
<i>Grassland and dry shrubland</i>	1	0		
<i>Savanna and dry woodland</i>	0.75	0		
<i>Desert</i>	1	0		
<i>Tundra</i>	0	1		
<i>weights</i>	0.5	0.5		
Bare Ground	Arctic/alpine			
<i>Desert</i>	0			
<i>Tundra</i>	1			
<i>weight</i>	1			

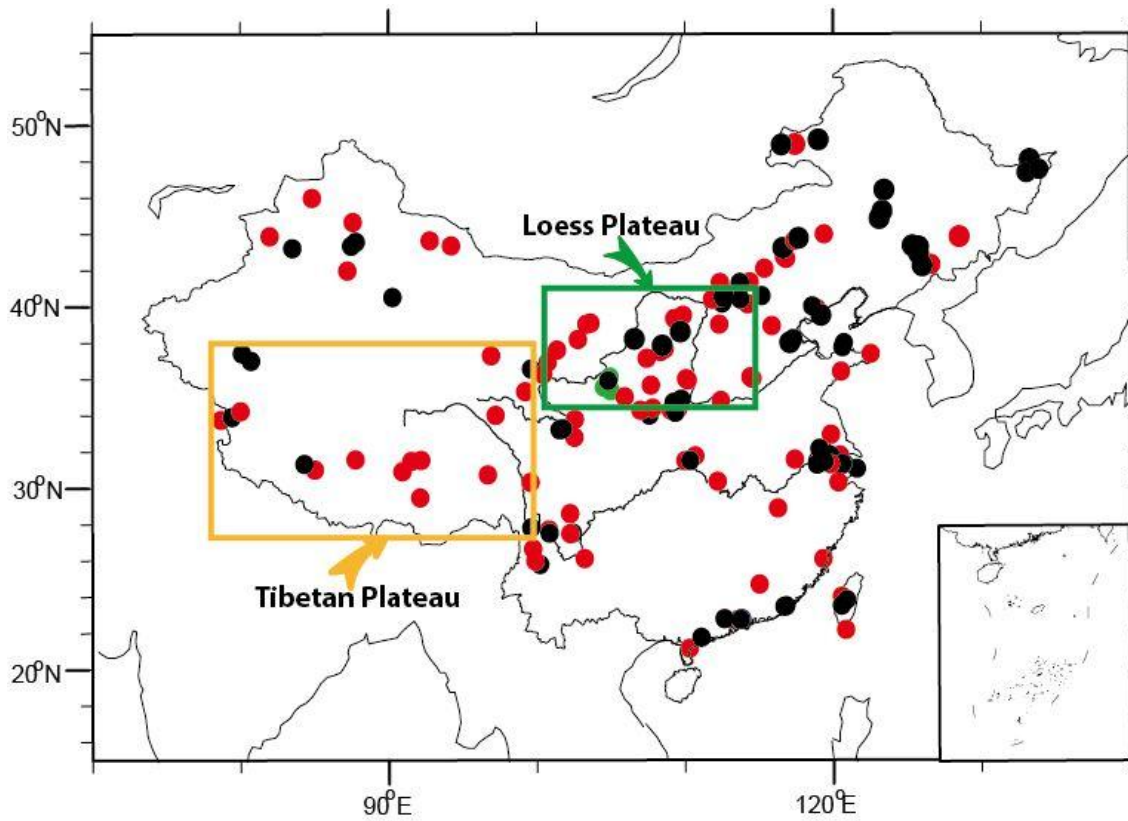
981

982 **Table 6. Regression coefficients between the reconstructed climates by inverse**
 983 **vegetation models and observed meteorological values**

Climate parameter	Slope	Intercept	R	ME	RMSE
MAT	0.82±0.02	0.92±0.18	0.89	0.16	3.25
MTCO (jan)	0.81±0.01	-1.79±0.18	0.95	-0.17	3.19
MTWA (jul)	0.75±0.03	4.57±0.60	0.75	-0.19	4.02
MAP	1.15±0.02	32.90±18.41	0.94	138.01	263.88
Pjan	1.01±0.02	0.32±0.47	0.94	0.52	8.89
Pjul	1.30±0.03	-21.67±4.52	0.89	16.45	52.9

984 The climatic parameters used for regression are the actual values. MAT annual mean
 985 temperature, MTCO mean temperature of the coldest month, MTWA mean temperature of the
 986 warmest month, MAP annual precipitation, RMSE the root-mean-square error of the residuals,
 987 ME mean error of the residuals, Pjan: precipitation of January, Pjul: precipitation of July, R is
 988 the correlation coefficient, ± stand error

989
 990
 991
 992
 993
 994
 995
 996
 997
 998
 999
 1000
 1001
 1002



1003

1004

1005 **Figure 1.** Distribution of pollen sites during mid-Holocene period in China. Black circle is the
 1006 original China Quaternary Pollen Database, red circles are digitized ones from published
 1007 papers, green circles represent the three original pollen data used in this study.

1008

1009

1010

1011

1012

1013

1014

1015

1016

1017

1018

1019

1020

1021

1022
1023
1024
1025
1026
1027
1028
1029
1030
1031
1032
1033
1034
1035
1036
1037
1038
1039
1040
1041
1042
1043
1044
1045
1046
1047
1048
1049
1050
1051

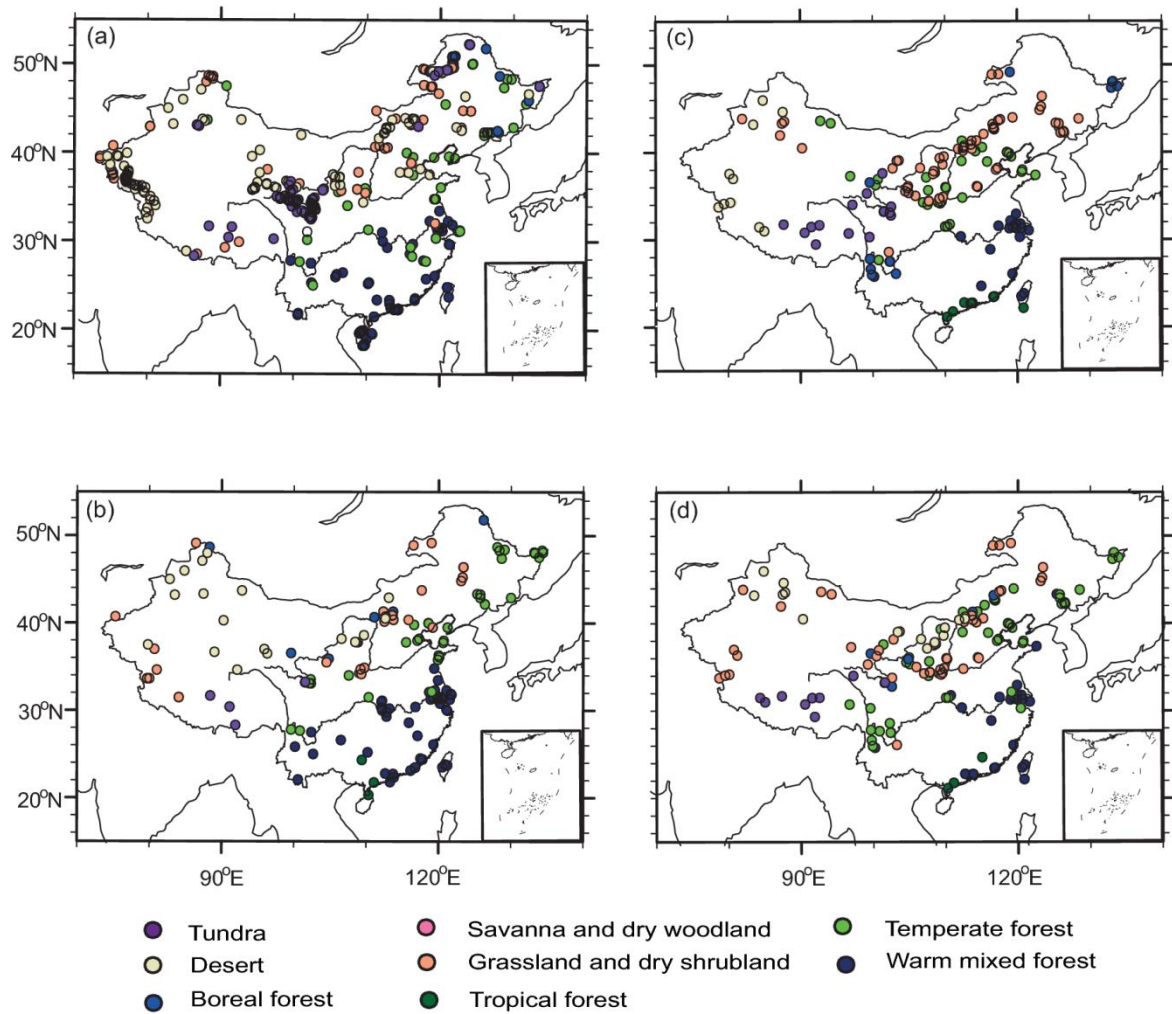
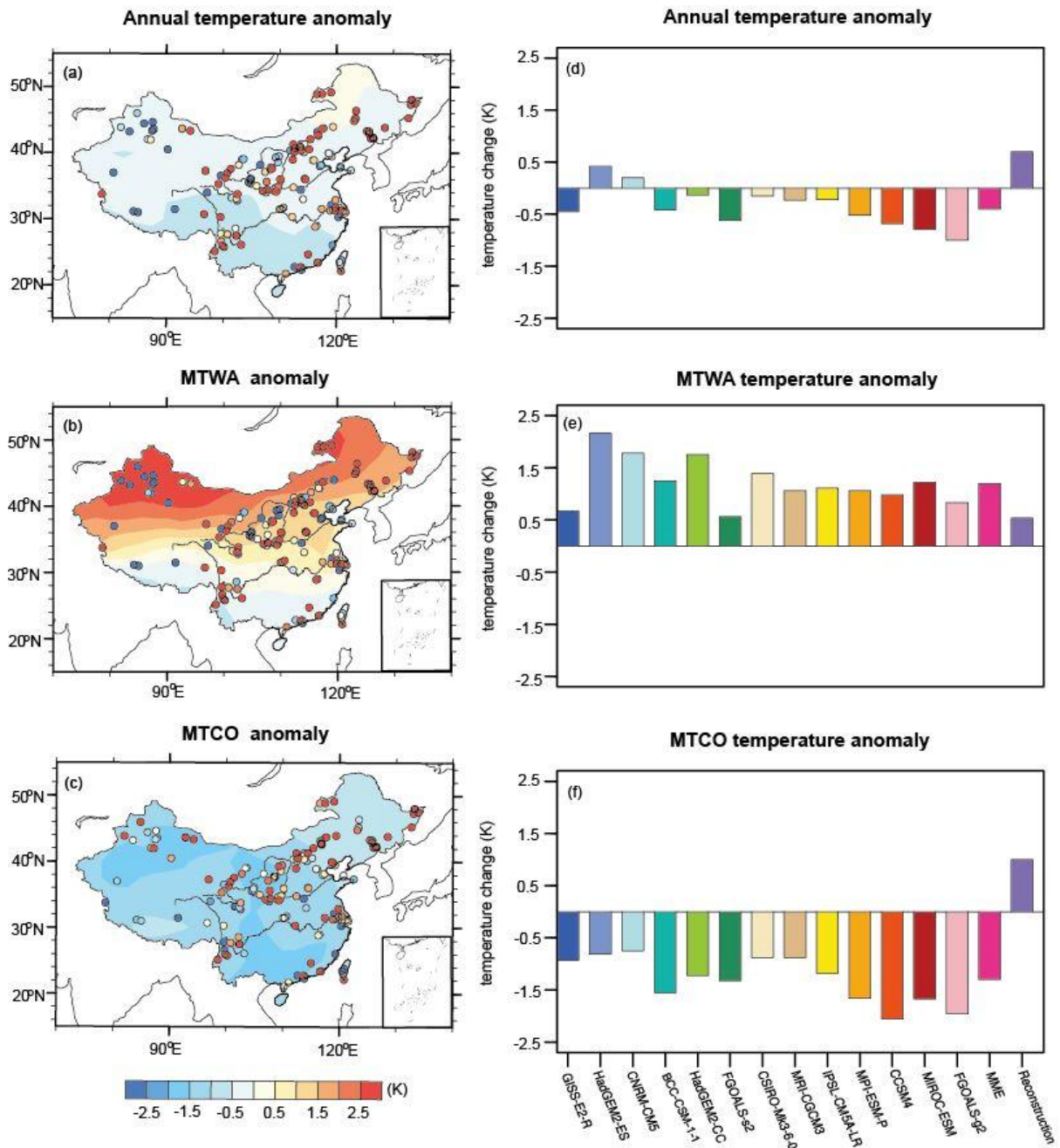


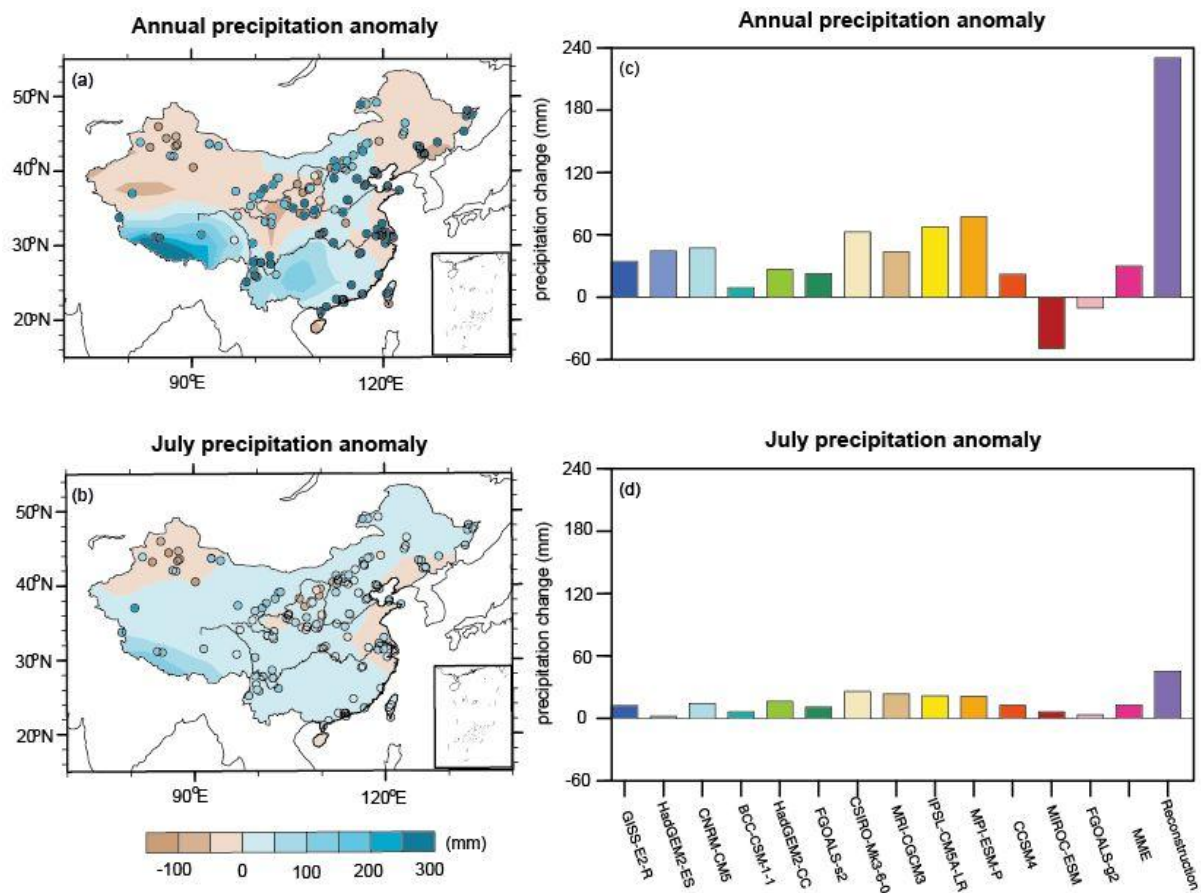
Figure 2. Comparison of megabiomes for PI (first row) and the MH (second row): (a,b) BIOME6000, (c,d) pollen data collected in this study.



1052
 1053 **Figure 3.** Model-data comparison for annual and seasonal (MTWA and MTCO) temperature
 1054 (K). For the left panel (a-c), points represent the reconstruction from IVM, shades show the
 1055 last 30-year means simulation results of multi-model ensemble (MME) for 13 PMIP3 models.
 1056 The grid mean value of temperature for each model, MME and reconstruction are also
 1057 displayed at the right panel (d-f).

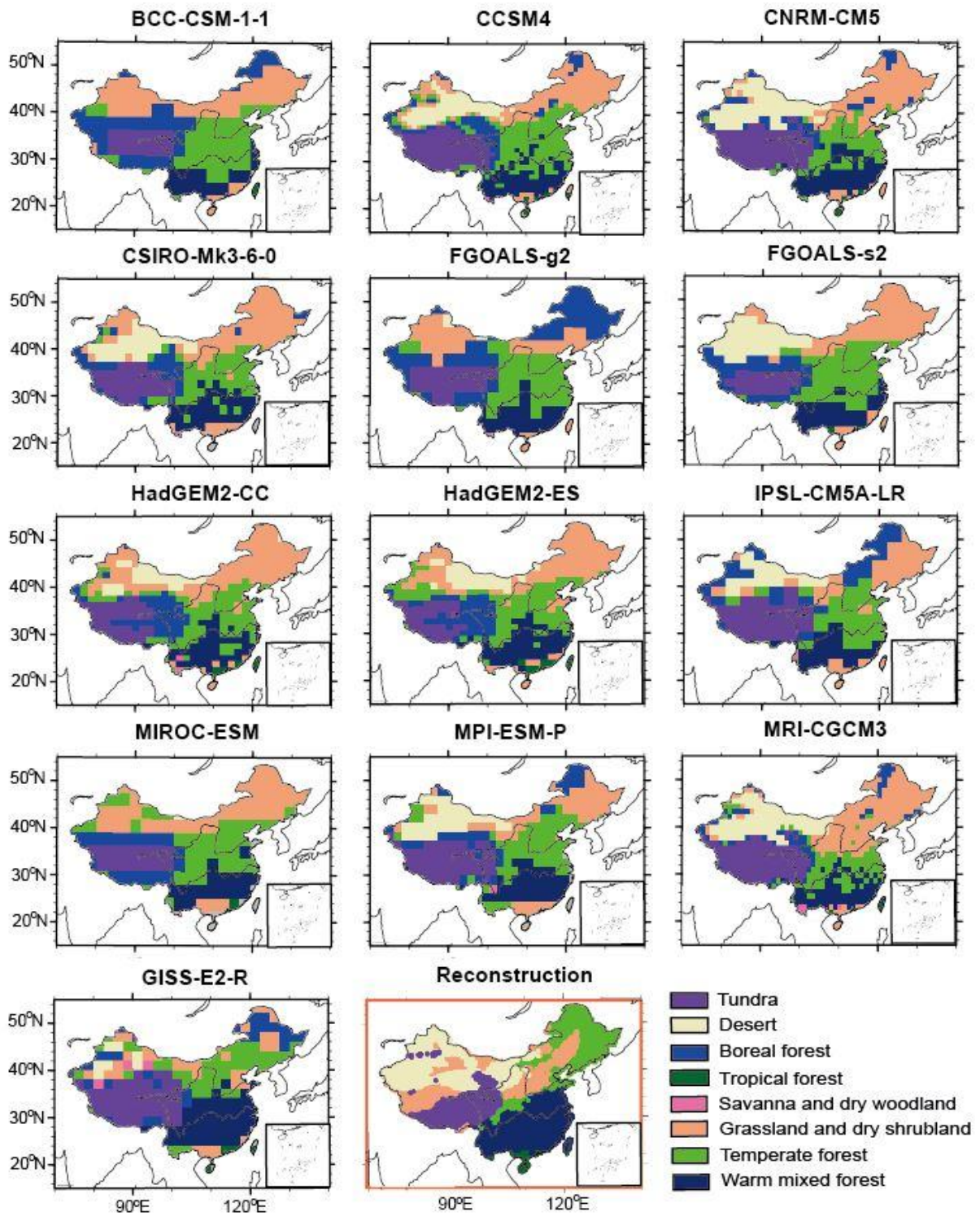
1058
 1059
 1060
 1061
 1062
 1063

1064
1065



1066
1067
1068
1069 **Figure 4.** Model-data comparison for annual and July precipitation (mm). For the left panel
1070 (a,b), points represent the reconstruction from IVM, shades show the last 30-year means
1071 simulation results of multi-model ensemble (MME) for 13 PMIP3 models. The grid mean
1072 value of precipitation for each model, MME and reconstruction are also displayed at the right
1073 panel (c,d).

1074
1075
1076
1077
1078
1079
1080
1081



1083

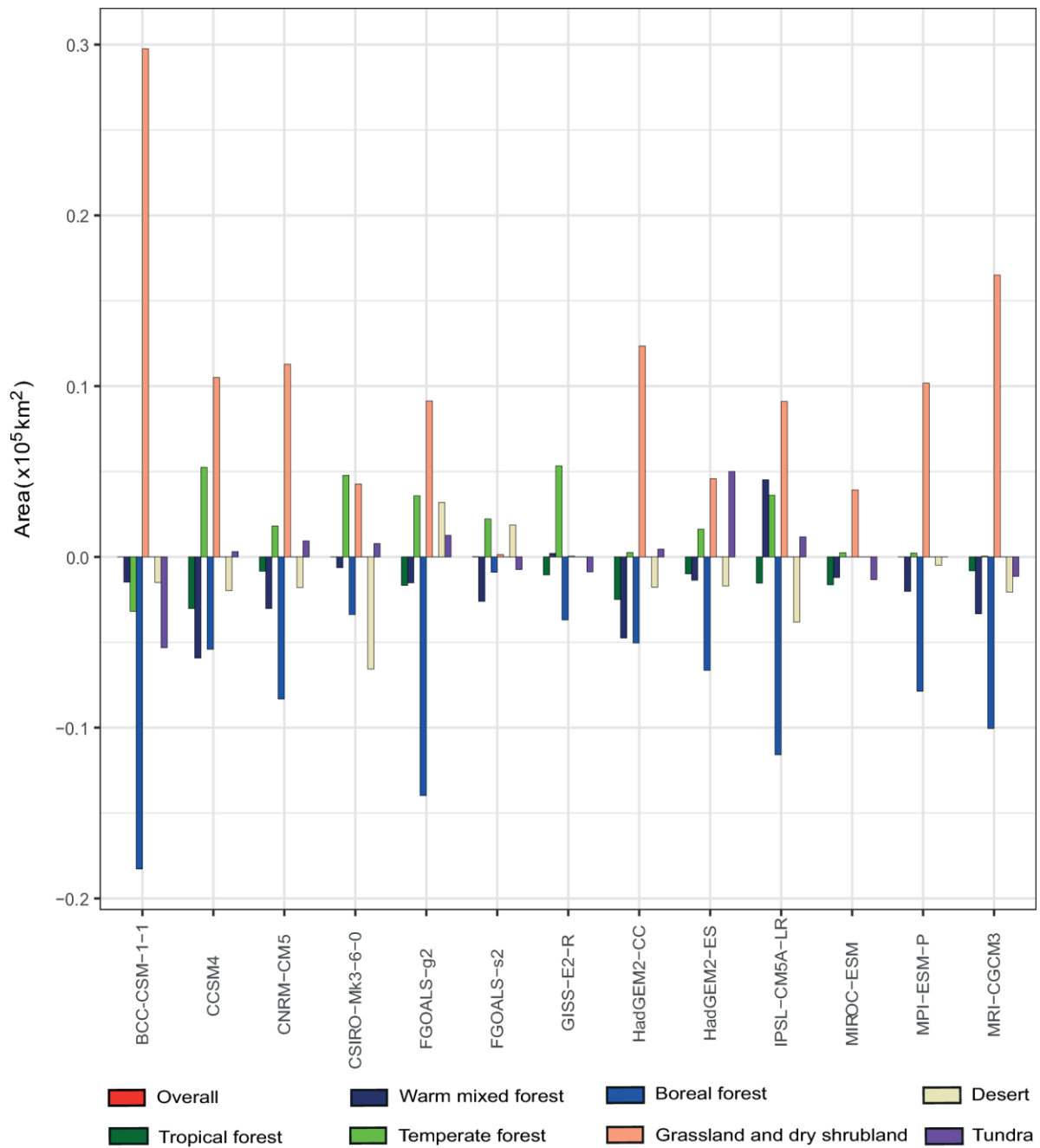
1084

1085 **Figure 5.** Comparison of interpolated megabiomes distribution (plot in red rectangle) with the
 1086 simulated spatial pattern from BIOME4 for each model during mid-Holocene.

1087

1088

1089
1090



1091
1092
1093
1094
1095
1096
1097
1098

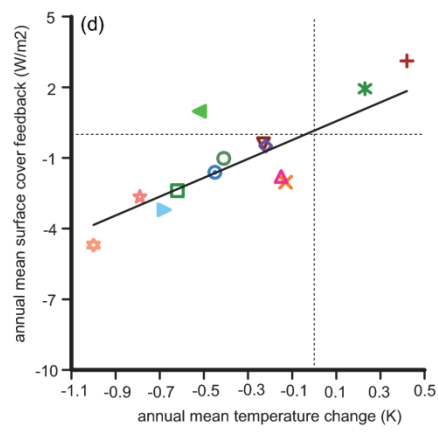
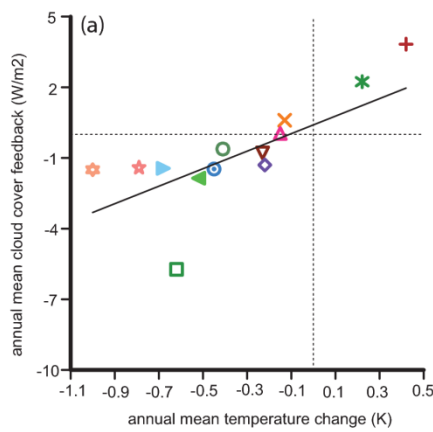
Figure 6. Changes in the extent of each megabiome as a consequence of simulated climate changes for each model, both expressed as change relative to the PI extent of same megabiome.

1099
1100

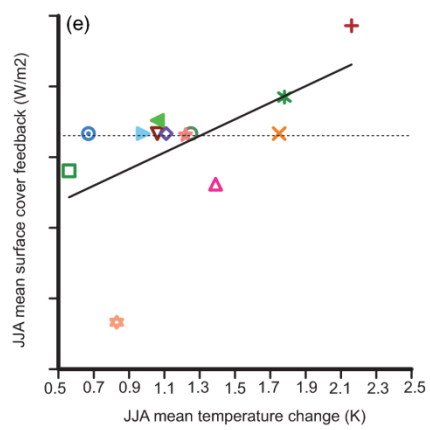
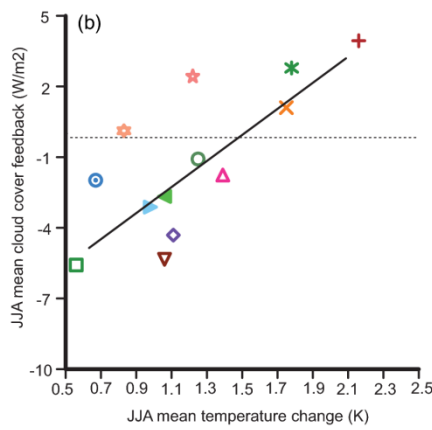
1101 **Figure 6.** Changes in the extent of each megabiome as a consequence of simulated climate
1102 changes for each model, both expressed as change relative to the PI extent of same
1103 megabiome.

1104
1105
1106
1107
1108
1109

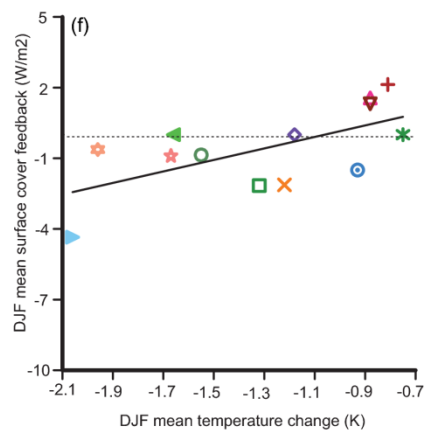
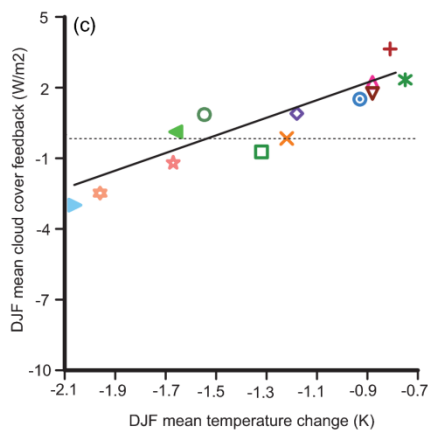
1110
1111
1112
1113
1114
1115
1116
1117



1118
1119
1120
1121
1122
1123
1124
1125



1126
1127
1128
1129
1130
1131



1132

1133

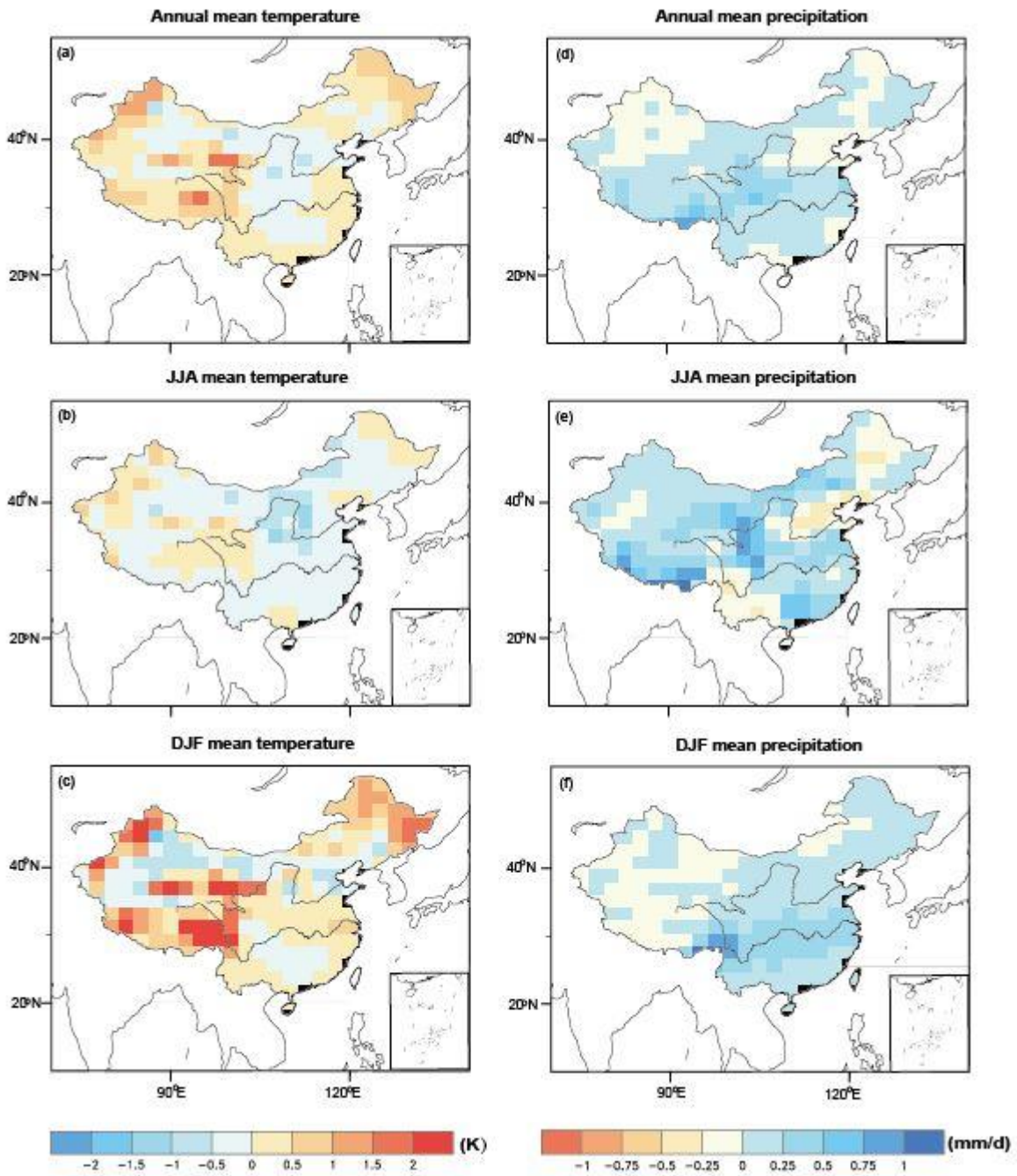
1134

1135

1136

1137 **Figure 7.** Scatter plots showing temperature, cloud cover feedback and surface albedo
1138 feedback changes during the MH. The values shown are the simulated 30-year mean anomaly
1139 (MH-PI) for the 13 models. **a**, annual mean temperature relative to the annual mean cloud
1140 cover feedback and **d**, annual surface albedo feedback. **b**, Summer (JJA) mean temperature
1141 relative to the summer mean cloud cover feedback and **e**, Summer surface albedo feedback.
1142 **c**, Winter (DJF) mean temperature relative to the summer mean cloud cover feedback and **f**,
1143 Winter surface albedo feedback. The horizontal and vertical lines in plots represent the value
1144 of 0.

1145



1146

1147 **Figure 8.** Climate anomalies between the two experiments (6 ka and 6 ka_VEG) conducted in
 1148 CESM version 1.0.5. The anomalies (6 ka_VEG-6 ka) of temperature and precipitation at
 1149 both annual and seasonal scale are presented, and all these climate variables are calculated as
 1150 the last 50-year means from two simulations.

1151